PL–TR–
94–3001

Theoretical Absorption Spectroscopy of High–Temperature Metal Vapors: Model and Experiment Compared

Jeffrey D. Mills

December 1994

Final Report

PHILLIPS LABORATORY
Propulsion Directorate
AIR FORCE MATERIEL COMMAND
EDWARDS AIR FORCE BASE CA 93524–7001

NOTICE

When U.S. Government drawings, specifications, or other data are used for any purpose other than a definitely related Government procurement operation, the fact that the Government may have formulated, furnished, or in any way supplied the said drawings, specifications, or other data, is not to be regarded by implication or otherwise, or in any way licensing the holder or any other person or corporation, or conveying any rights or permission to manufacture, use or sell any patented invention that may be related thereto.

FOREWORD

The work reported in this interim report was performed by Jeff Mills, Indiana University, under JON: 2308M1R1 with the OLAC PL/RKFE Branch at the Phillips Laboratory, Edwards AFB CA 93524–7680. OLAC PL Project Manager was Dr. C. William Larson.

This report has been reviewed and is approved for release and distribution in accordance with the distribution statement on the cover and on the SF Form 298.

C. WILLIAM LARSON
Project Manager

RANNEY G. ADAMS
Public Affairs Director

TIMOTHY A. MCKELVEY, Major, USAF
Acting Director,
Fundamental Technologies Division

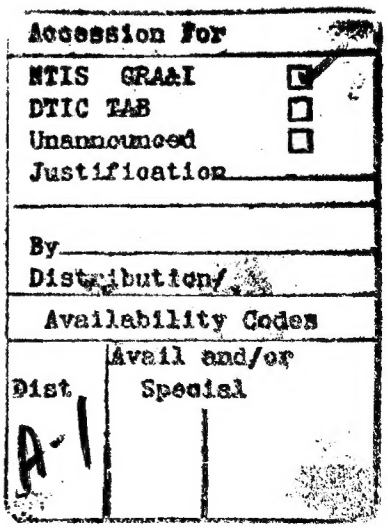

REPORT DOCUMENTATION PAGE

Form Approved
OMB No 0704-0188

1. AGENCY USE ONLY (LEAVE BLANK)	2. REPORT DATE	3. REPORT TYPE AND DATES COVERED
	December 1994	Final Report

4. TITLE AND SUBTITLE
Theoretical Absorption Spectroscopy of High-Temperature Metal Vapors: Model and Experiment Compared

5. FUNDING NUMBERS
C:
PE:
PR: 2308
TA: M3RI

6. AUTHOR(S)
Jeffrey D. Mills

7. PERFORMING ORGANIZATION NAME(S) AND ADDRESS(ES)
Phillips Laboratory
OLAC PL/RKFE
9 Antares Road
Edwards AFB CA 93524-7680

8. PERFORMING ORGANIZATION REPORT NUMBER
PL-TR-94-3001

9. SPONSORING/MONITORING AGENCY NAME(S) AND ADDRESS(ES)

10. SPONSORING/MONITORING AGENCY REPORT NUMBER

11. SUPPLEMENTARY NOTES

COSATI CODE(S):

12a. DISTRIBUTION/AVAILABILITY STATEMENT
Approved for Public Release; Distribution is Unlimited

12b. DISTRIBUTION CODE
A

13. ABSTRACT (MAXIMUM 200 WORDS)

Theoretical calculations in support of absorption spectroscopy of buffered metallic vapors in the Plasma Spectroscopy Cell are described. After a brief exposition of the theoretical principles and ingredients of the quantum-mechanical, state-to-state treatment of transition processes in atoms and diatoms at thermodynamic equilibrium, various aspects of the model and experimental absorption spectra for the lithium system are compared and discussed. Special emphasis is given to outlining those spectral characteristics which are most relevant to the energy transfer properties of the sample but are as yet incompletely understood and to determining the minimal computational algorithm sufficient to rapidly and accurately calculate absorption by these materials. An account of the modelling of the aluminum/lithium system preparative to a search for a heretofore unobserved molecule, aluminum lithium, is also included.

14. SUBJECT TERMS
solar plasma propulsion; high temperature lithium spectroscopy; high temperature sodium spectroscopy; alkali metal vapor spectroscopy

15. NUMBER OF PAGES

16. PRICE CODE

17. SECURITY CLASSIFICATION OF REPORT	18. SECURITY CLASSIFICATION OF THIS PAGE	19. SECURITY CLASSIFICATION OF ABSTRACT	20. LIMITATION OF ABSTRACT
Unclassified	Unclassified	Unclassified	SAR

CONTENTS

CONTENTS

I. Introduction[1]

Of the many optical processes manifested in material samples, absorption of light is among the most fundamental and in many cases is treated with sufficient accuracy by a quantum mechanical theory which involves induced single-step transitions between states of the composite atoms and molecules. In this work such microscopic, theoretical considerations are applied to calculating the macroscopic absorption by the atoms and diatomic molecules of high-temperature metal vapors of the type countenanced as energy collection and transfer fluids in high-energy-density-propulsion and solar-power-conversion devices. In particular, it should be emphasized that the absolute absorption (and by extension, the emission which can easily be derived from it) by equilibrated, multicomponent samples of finite extent is the ultimate subject of interest, rather than mere band shapes or relative absorption intensities due to one particular species. This is motivated by the critical dependence of the overall radiative and thermal properties of an extended sample upon the quantitative spatial and spectral dependence of its absorptivity and emissivity.[2] Thus, a model exact enough to describe all of these characteristics and yet simple and general enough to allow facile calculation for a variety of thermodynamic conditions and chemical species would seem to be especially useful. In the pursuit of such economy, application of the outlined theoretical framework to experimental investigations of two classes of chemical systems, one relatively simple and well characterized, and the other including spectroscopically rich and novel chemical species, is accompanied by an examination of the justification and implications of several common and useful approximations. Included is a brief description of how this spectral modelling can be extended in an effort to characterize the overall thermal and radiative transport properties of real materials important for practical applications.

II. Theoretical Background

[1] The author would like to gratefully acknowledge the contributions of others who made this work possible: Dr. C. William Larson manages the project under which this investigation was undertaken and was a source of many invaluable ideas; research advisor, Prof. Peter W. Langhoff, provided the impetus for and gave freely of his time in working out the details of this approach; Paul Erdman had a large part in the experimental measurements described, as did Dr. Mario Fajardo and Dr. Patrick Carrick; Prof. W.C. Stwalley provided unpublished results and some of the computer programs employed; Dr. Marcy Rosenkrantz and Dr. Daniel Konowalow contributed unpublished results and were a valuable resource in understanding the *ab initio* calculations; and Drs. S.R. Langhoff and C.H. Bauschlicher provided additional results relative to their published work. Financial support during this investigation was provided by Indiana University and the 1993 Summer Research Program of the Air Force Office of Scientific Research.

[2] The greenhouse-type trapping of thermal radiation by planetary atmospheres with different optical response in different regions of the spectrum provides a simple example of this phenomenon. In a flowing, absorbent vapor these sorts of effects are thought to allow unusual temperature and concentration profiles which are critical for the efficiency of power-conversion devices.

The theoretical description and derivation of the various relations between the molecular and atomic properties required to account for the absolute one-photon absorption of gaseous atomic and diatomic samples has been outlined in detail elsewhere.[3] Briefly, the goal is to calculate the transmission of light,

$$\frac{I(\nu)}{I_0(\nu)} \equiv T(\nu) = e^{-k(\nu)\Delta x}, \tag{1}$$

through a uniform[4] equilibrated sample of length, Δx, at wavelengths across the entire visible spectrum. In the nondispersive limit the absorption coefficient is composed linearly of terms for all particle types present, as:

$$k(\nu) = \sum_{\substack{q \\ \text{species}}} \sigma_q(\nu)\left(\frac{N}{V}\right)_q. \tag{2}$$

Both the intrinsic per molecule (or atom) optical absorption cross section, $\sigma_q(\nu)$, which allows the connection between the macroscopic, measurable optical properties of a sample and the microscopic characteristics of its constituent chemical species, and the extrinsic number density, $\left(\frac{N}{V}\right)_q$, of each of these species can be described in several levels of approximation and are treated in turn in what follows.

A. Absorption by Atoms

For atoms the energy-dependent absorption cross section is given by a sum over transitions between initial and final levels, I and F, of degenerate states, as:[5,6]

$$\begin{aligned}\sigma_q(E) &= \tfrac{2\pi^2 e^2 \hbar}{mc} \sum_{I,F} f_{IF} \frac{\left(\frac{N}{V}\right)_I}{\left(\frac{N}{V}\right)_q} \phi_{IF}(E) \\ &= \sum_{I,F} \sigma_{IF} \frac{\left(\frac{N}{V}\right)_I}{\left(\frac{N}{V}\right)_q} \phi_{IF}(E).\end{aligned} \tag{3}$$

---

[3] J.D. Mills, *Extended C500 Research Report,* Indiana University, May 1992 and references cited therein.

[4] For nonuniform samples the transmission is still fundamentally determined by the now spatially dependent absorption coefficient. So long as the samples are locally equilibrated with known spatial temperature and concentration distributions, the absorption coefficient can be calculated within the present framework for each point in the sample. The total transmission is then an accumulation of the effects of all parts of the sample. Motivated by a desire to focus on the means of constructing the absorption coefficient from microscopic, theoretical considerations, this report contains only transmission spectra of samples assumed to be uniform.

[5] S.M. Blinder, *Foundations of Quantum Dynamics*, (Academic, London, 1974), pp. 190-200.

[6] J.I. Steinfeld, *Molecules and Radiation,* Second Ed., (MIT Press, Cambridge, MA, 1986), pp. 25-30.

Here f_{IF}, the oscillator strength, is the per atom combined strength of transitions from an average state of the lower level to all states of the final level and is simply the number of electrons nominally involved in such a process. For the sake of notational simplicity the species dependence is considered to be implicit in the level and state indices in this and following equations. The density of atoms, $(\frac{N}{V})_I$, in the initial level relative to the total species density (the Boltzmann level population fraction) is given by statistical mechanics, as:

$$\frac{(\frac{N}{V})_I}{(\frac{N}{V})_q} = \frac{g_I\, e^{-E_I/k_B T}}{\sum_K g_K\, e^{-E_K/k_B T}} \tag{4}$$

in terms of the energies, E, and degeneracies, g, of the levels and the temperature, T, of the absorbing sample. Finally, in a form which will subsequently prove to be convenient, the later part of equation (3) expresses the total energy-dependent absorption cross section in terms of an energy-integrated level-to-level absorption cross section, σ_{IF}, which contains all the intrinsic strength information for a transition peak, a population fraction, and $\phi_{IF}(E)$, the unity-normalized lineshape function between levels, which contains the overall distribution of transition intensity around the root transition energy.

B. Absorption by Diatoms

For diatomic molecules, approximations of varying sophistication and utility are convenient or necessary in constructing the intrinsic absorption cross section and these are outlined in application to bound-bound and bound-free transitions.

1. Vibronic Resolution

At the simplest level, molecular transitions between bound electronic, vibrational, and rotational states can be grouped in such a way that those with the same nominal electronic and vibrational character are considered to occur around a common, effective transition energy. This leads to a molecular absorption cross section independent of rotational degrees of freedom:

$$\sigma_q(E) = \frac{2\pi^2 e^2 \hbar}{mc} \sum_{\epsilon_I, \epsilon_F} \bar{f}^{abs}_{\epsilon_I \epsilon_F} \sum_{v_I, v_F} \chi_{v_i, v_f} \frac{\bar{E}_{IF}}{\bar{E}^{abs}_{\epsilon_I \epsilon_F}} \frac{(\frac{N}{V})_I}{(\frac{N}{V})_q} \phi_{vbr,IF}(E). \tag{5}$$

Here i and f denote individual states in the initial and final levels and the relative strength, χ_{v_i,v_f} (in the eponymous approximation, a Franck-Condon factor), of a transition of energy, $\bar{E}_{IF}$, between what can be thought of as singly (or at least identically) degenerate vibronic levels is notated so as to emphasize its calculation from two individual state wave functions representing the averaged electronic-vibrational levels denoted by ϵ and v. Likewise $\bar{f}^{abs}_{\epsilon_I \epsilon_F}$ and $\bar{E}^{abs}_{\epsilon_I \epsilon_F}$ can be thought of as the overall oscillator strength and average transition energy for the entire electronic transition band. The most accurate vibronic lineshape function, $\phi_{vbr,IF}(E)$, would contain all

the information about rotational state distribution in an individual vibronic band. In an effort to economically account for the crudest effects of this spectral distribution, this lineshape function can be approximated by a simple, symmetric profile with an effective width taken to be the same for all vibronic peaks in an electronic band. For the purposes of even simpler illustration, the lineshape function and the total vibronic strength can be replaced by a simple stick or spike with height proportional to the transition propensity.

For absorption processes involving an initial bound and final unbound state, the cross section takes a similar form:

$$\sigma_q(E) = \frac{2\pi^2 e^2 \hbar}{mc} \sum_{\epsilon_I, \epsilon_F} \bar{f}^{abs}_{\epsilon_I \epsilon_F} \sum_{v_I} \chi_{v_i}(E) \frac{\overline{E}_{IF}}{\overline{E}^{abs}_{\epsilon_I \epsilon_F}} \frac{(\frac{N}{V})_I}{(\frac{N}{V})_q} \tag{6}$$

but has the lineshape and strength factor combined in a strength function which varies continuously with transition energy because of the continuum nature of the final state.

2. Rovibronic Resolution

In more exact treatments the rotational structure of transition bands must be included. At the most extensive level still consistent with the Born-Oppenheimer Approximation, bound-bound transitions with energy and strength both fully dependent upon the individual rovibronic levels are considered as:

$$\sigma_q(E) = -\frac{2\pi^2 e^2 \hbar}{mc} \sum_{\epsilon_I, \epsilon_F} \bar{f}^{abs}_{\epsilon_I \epsilon_F} \sum_{v_I, v_F} \sum_{J_I, J_F} \chi_{v_i J_i, v_f J_f} \frac{E_{IF}}{\overline{E}^{abs}_{\epsilon_I \epsilon_F}} \xi^{rot}_{J_I J_F} \frac{(\frac{N}{V})_I}{(\frac{N}{V})_q} \phi_{rvbr,IF}(E) \tag{7}$$

where the strength factors are calculated for representative states of the rovibronic level-to-level manifold and $\xi^{rot}_{J_I J_F}$, the known Hönl-London factors specific to the symmetry of the electronic transition, account for the angular momentum degeneracies and transition selection rules between the states of the levels and have been normalized to the initial level degeneracy, $2J_I + 1$. The state-dependent and electronic-band-averaged transition energies and strengths are denoted as before. At this level one of the familiar transition-peak distribution functions, suitably broadened to account for the existent molecular environment, can be more comfortably used as the lineshape function for an individual rovibronic transition. Practical limitations and ignorance of its dependence upon initial and final state often necessitate use of a distribution function identical for all transitions of a molecular species. Finally, for bound-bound absorption it is clear that the total cross section of equation (7) (and indeed that for the vibronic case of eq. (5)) can be composed as a sum over products of integrated level-to-level cross sections, population fractions, and energy-dependent lineshapes to yield an expression analogous to the later part of equation (3).

The strength factors used in equation (7) and the previous pair of equations are of two customary types. Franck-Condon factors are calculated assuming that the

transition dipole does not vary from an average value over the vibrational coordinate of the molecule. This approximation will be shown to be sufficient for only some molecular transitions. More exact strength factors can be derived by including the dependence upon internuclear separation, but ignorance of the transition moment function sometimes prohibits their construction.

An additional simplification can be made if the transition strengths fully dependent upon rotational degrees of freedom are replaced with a set identical for all states within a given vibronic manifold. This yields a hybrid treatment with vibronic strengths applied to transitions between states with energies fully dependent upon rotational degrees of freedom. This approximation is accompanied by significant resource savings and can be quite accurate.

As for the vibronic case (*c.f.* eqn. (6)), the bound-free absorption cross section which includes rotational degrees of freedom:

$$\sigma_q(E) = -\frac{2\pi^2 e^2 \hbar}{mc} \sum_{\epsilon_I, \epsilon_F} \bar{f}^{abs}_{\epsilon_I \epsilon_F} \sum_{v_I} \sum_{J_I, J_F} \chi_{v_i J_i, J_f}(E) \frac{E_{IF}}{\bar{E}^{abs}_{\epsilon_I \epsilon_F}} \xi^{rot}_{J_I J_F} \frac{(\frac{N}{V})_I}{(\frac{N}{V})_q} \tag{8}$$

can be composed in terms of a transition strength function which is a continuously varying function of energy.

3. Intrinsic Molecular Parameters

Much of the atomic and molecular information necessary for the calculation of the intrinsic absorption cross section has been published and is suitable for straightforward application. Selection and incorporation of this data is discussed in the section describing spectroscopic modelling of specific chemical systems. On the other hand, the determination of molecular state energies and combined strength factors from Born-Oppenheimer potential energy curves and transition dipole moments involves separate calculation and is thus outlined here briefly.

The rotationally dependent molecular states and their energies are obtained as the vibrational eigenfunctions, $\phi_{v,J}$, and eigenvalues, $E_{v,J}$ of the one-dimensional radial Schrödinger Equation for molecular vibration:

$$-\frac{\hbar^2}{2\mu}\frac{d^2}{dR^2}\phi_{v,J} + \left[E_{v,J} - U_J(R)\right]\phi_{v,J} = 0 \tag{9}$$

in which the effective internuclear potential, $U_J(R)$, includes centrifugal effects and is given in terms of its rotationless Born-Oppenheimer counterpart, $V^{BO}(R)$, taken from either experiment or calculation and the total electronic angular momentum, Ω, by:

$$U_J(R) = V^{BO}(R) + \frac{\hbar^2}{2\mu R^2}\left[J(J+1) - \Omega^2\right]. \tag{10}$$

Once obtained, the energies give the rovibronic level population fractions by the familiar expressions of statistical mechanics:

$$\frac{(\frac{N}{V})_I}{(\frac{N}{V})_q} = \frac{g_{\epsilon_I}(2J_I+1)\, g_I^{ns}\, e^{-E_I/k_B T}}{\sum_K g_{\epsilon_K}(2J_K+1)\, g_K^{ns}\, e^{-E_K/k_B T}} \tag{11}$$

where g_ϵ, $(2J+1)$, and g^{ns} are the electronic, angular momentum, and nuclear spin degeneracies, respectively. An analogous expression in terms of effective vibrational level energies but without dependence upon rotational or nuclear spin degeneracies exists for the vibronic case.

The total absorption strength due to a level-to-level transition can be considered to be composed of three parts: the relative strength of a single state-to-state representative of the manifold of transitions, the Hönl-London factor providing the weighting factor of such a transition in the level-to-level manifold, and the overall strength associated with the electronic band. The first of these is provided by integrals over the initial and final vibrational eigenstates determined in equation (9). Franck-Condon factors are simply the square of the overlap of initial and final vibrational eigenfunctions:

$$\chi^{FCF}_{v_i J_i, v_f J_f} = \left| \langle \phi_{v_i J_i} \mid \phi_{v_f J_f} \rangle \right|^2 \tag{12}$$

and the analogous factors including the internuclear-separation dependence of the transition strength are given in terms of the appropriate matrix elements according to:

$$\chi^{\mu}_{v_i J_i, v_f J_f} = \frac{\left| \langle \phi_{v_i J_i} | \, \vec{\mu}_{if}(R) \, | \phi_{v_f J_f} \rangle \right|^2}{|\vec{\mu}_{if}(R_{e,i})|^2}. \tag{13}$$

For most systems the Born-Oppenheimer transition dipole moment, $\vec{\mu}_{if}(R)$, between initial and final electronic states is most accurately given by *ab initio* electronic structure calculations for most systems. The equilibrium separation of the initial state, $R_{e,i}$, not only defines an average value for the transition dipole consistent with predominant thermal state populations, but also can be used to parameterize the overall absorption oscillator strength of an electronic band in the familiar expression:[7]

$$\bar{f}^{abs}_{\epsilon_I \epsilon_F} = \frac{2mE_{if}(R_{e,i})}{3e^2\hbar^2 g_I} |\vec{\mu}_{if}(R_{e,i})|^2, \tag{14}$$

where the vertical transition energy, $E_{if}(R_{e,i})$, the energy difference between the two potential energy curves at the initial state equilibrium separation, serves as the root transition energy denoted by $\bar{E}^{abs}_{\epsilon_I \epsilon_F}$ previously.

The arduousness of the calculation and inclusion of this full set of transition strengths and energies provides the main impediment to rapid calculation of spectra in the present computational framework and thus motivates further simplifications or approximations which involve extracting average or effective energies or strengths from among this more complete rovibronic set. Separate technical difficulties are associated with the continuously varying state energy of unbound potentials. As these are not considered fundamental to the present framework, discussion of their solution is deferred until they become important in the spectral modelling.

---

[7] S.M. Blinder, *op. cit.*, pp. 198-200.

C. Bulk Thermodynamic Parameters

Having described the construction of per atom or molecule absorption cross sections, calculation of the total sample absorption coefficient via equation (2) requires only the specification of the particle densities of all species. The absorbing milieu is assumed to be composed of free atoms, $p \in \{A, B, C, \ldots\}$, as well as molecules, m, which can be thought of as being formed from two, or in this general treatment even more, of these atoms according to the elementary reactions:

$$\nu_{A,m}\,A + \nu_{B,m}\,B + \nu_{C,m}\,C + \ldots \rightleftharpoons A_{\nu_{A,m}} B_{\nu_{B,m}} C_{\nu_{C,m}} \cdots \tag{15}$$

where $\nu_{p,m}$ is the stoichiometric coefficient for each atom in a molecule. If the total atomic particle density, $\left(\frac{N}{V}\right)_{p,tot}$, present in the absorbing gas in the form of both atoms and molecules can be determined from some thermodynamic initial conditions, the expression for the mass conservation of each atom,

$$\left(\frac{N}{V}\right)_p + \sum_{\substack{m \\ mol.}} \nu_{p,m} \left(\frac{N}{V}\right)_m = \left(\frac{N}{V}\right)_{p,tot}, \tag{16}$$

and the molecular equilibrium constants,

$$K_m = \frac{\left(\frac{N}{V}\right)_m}{\prod\limits_{\substack{p \\ atoms}} \left[\left(\frac{N}{V}\right)_p\right]^{\nu_{p,m}}} \tag{17}$$

$$\left(e.g. \qquad K_{AlLi} = \frac{\left(\frac{N}{V}\right)_{AlLi}}{\left(\frac{N}{V}\right)_{Al}\left(\frac{N}{V}\right)_{Li}} \right),$$

provide an equation of constraint for each chemical species in the equilibrated mixture. Solution of these simultaneous equations thus defines the existent particle densities. Although the equilibrium constants of some common molecular systems have been measured and reported, it was discovered that these values are often more accurately determined using chemical statistical mechanics, as:

$$K_m = \frac{\left(\frac{Q_m^{mol}}{V}\right)}{\prod\limits_{\substack{p \\ atoms}} \left(\frac{Q_p^{atom}}{V}\right)^{\nu_{p,m}}} \tag{18}$$

where the atomic and diatomic rovibronic partition functions are given by direct summation over levels,

$$Q_p^{atom} = V\left(\frac{2\pi m_p k_B T}{h^2}\right)^{\frac{3}{2}} \sum_K g_K\, e^{-E_K/k_B T} \tag{19}$$

$$Q_p^{mol} = V\left(\frac{2\pi m_m k_B T}{h^2}\right)^{\frac{3}{2}} \sum_{\epsilon_K v_K J_K} g_{\epsilon_K} (2J_K + 1)\, g_K^{ns}\, e^{-E_K/k_B T}, \qquad (20)$$

a similar expression can be constructed for the vibronic approximation, and the level degeneracies and energies have been previously described.

It should be emphasized that by combining both elements of equation (2), the per atom or molecule absorption cross section and the particle densities of each species in the observation zone, the optical absorption of an arbitrary mixture of atomic and diatomic absorbers can be quantitatively predicted with no dependence upon arbitrary factors or information outside the thermodynamics or quantum mechanics of the system. Much of the discussion which follows is motivated by the desire to define the essential features of the minimal procedural schema required to successfully accomplish this task in different materials with transitions of varying character. In particular, in the context of more clearly identifying the specific ingredients which go into the theoretical framework, the effect and utility of various approximations used in constructing these parameters will be gauged by comparing model and experimental spectra. Before proceeding with this discussion of the results of applying the theoretical framework, there is a brief discussion of two other optical properties which are derived with ease from the absorption cross section and may be useful in further understanding these samples.

D. Other Optical Properties

One-photon absorption is but one of the many optical processes possible in physical samples. The one-photon spontaneous emission and the two-photon elastic (Rayleigh) scattering responsible for the refractive index can also be derived from the preceeding theoretical framework. Research is currently underway to compare these modelled properties with what is measured and confirm their value in characterizing optical samples.

1. Spontaneous Emission

Atoms and molecules in an equilibrated spectroscopic sample statistically, if sparsely, populate excited states and in a process time-reversed with respect to absorption, can spontaneously emit a single photon and fall to a state in a lower-energy level. By carefully considering the relative equilibrium populations of the reversed initial (F) and final (I) levels, the intensity emitted in all directions at photon energy, E, can be constructed as:[8]

$$I_{em}(E) = \frac{2E^3}{h^2c^2} \sum_q N_q \sum_{IF} \frac{g_I}{g_F} \frac{(\frac{N}{V})_F}{(\frac{N}{V})_q} \frac{E}{E_{IF}} \sigma_{IF}\, \phi_{FI}(E) \qquad (21)$$

where N_q is the total number of particles of a particular species, g represents the total level degeneracies, and $\phi_{FI}(E)$ is a lineshape function which contains all the

[8] J.I. Steinfeld, *op. cit.*, pp. 25-30.

frequency dependence of a transition and is identical for absorption and emission. The symmetric nature of absorption and emission can be seen in the inclusion of σ_{IF}, the integrated vibronic or rovibronic level-to-level absorption cross section. Accurate modelling of this spectral characteristic will allow the energy transfer properties of realistic absorbing and emitting samples of finite extent to be more accurately predicted.[9]

2. Dispersion of Light

The dispersion of light, the phenomenon responsible for the refractive index, can be determined in a manner similarly dependent upon the absorption cross section. In the limit of low dispersion, classical electromagnetic theory[10,11] allows the bulk frequency-dependent refractive index, $n(\nu)$, to be expressed in terms of the intrinsic atomic or isotropic molecular polarizabilities, $\alpha_q(\nu)$, as:

$$n(\nu) - 1 = 2\pi \sum_{\substack{q \\ \text{species}}} \alpha_q(\nu)\left(\frac{N}{V}\right)_q. \tag{22}$$

The polarizability can then be constructed from the level-to-level absorption cross sections as:

$$\alpha_q(E) = \frac{hc}{4\pi} \sum_{IF} \frac{\sigma_{IF}}{E_{IF}} \tilde{\phi}_{IF}(E) \tag{23}$$

where $\tilde{\phi}_{IF}(E)$ is the dispersion analogue of the absorption lineshape and reflects the close connection between the in-phase polarization/dispersion response and the out-of-phase absorption signal. That a measurement of the refractive index can be invaluable in characterizing the detailed frequency dependence of optical absorption, especially the intensity profile of a collection of molecular lines, will be pointed out subsequently.

III. Results and Discussion of Completed Work

Coupled with a tractable computational algorithm, the theoretical framework just described is used to interpret and predict the results of optical absorption by metal vapors in the Plasma Spectroscopy Cell (PSC) at Phillips Laboratory, Edwards Air Force Base. An extensive description of the capabilities and character-

[9] The microscopic theoretical approach used here has a macroscopic counterpart in the theory of radiative transport. The assimilation of Kirchoff's Law into the present approach may allow insight into the proper means of accounting for coincident emission and absorption. Failure to do so has been found to cause difficulties in comparing experimental emission spectra with those modelled in the present framework. This and other related topics are discussed in the work cited as reference 13.

[10] S.A. Korff and G. Breit, *Rev. Mod. Phys.*, 4, 471 (1932).

[11] F. Wooten, *Optical Properties of Solids*, (Academic, New York, 1972), pp. 42-84.

istics of this apparatus has been previously published.[12,13] Briefly, it is comprised of a large containment vessel equipped to prepare and allow spectroscopic investigation of high-temperature (up to 2200K) and high-pressure (by design, up to 100 atm.) metal vapors. Inside, rare-gas-buffered vapors evaporate from condensed phases of the pure metals which are held at fixed, known temperatures and these vapors are allowed to mix under thermodynamic conditions in which chemical equilibrium is rapidly attained. Carefully shielded windows then allow the slowly and continuously flowing mixtures to be interrogated by light sources of various types.

The calculations described are performed on VAX computers at Indiana University and the CRAY-YMP computer at the University of Nevada–Las Vegas. Times to generate spectra fall in the range of seconds to hours, while the one-time generation of strength factors requires up to a week of computer time.

There follows an account of the application of the theoretical framework to two types of systems. The simple, pseudo-one-electron alkali metals and their dimers are not only interesting because of their potential applications, but also provide a good test of the accuracy and applicability of the method and the approximations expedient therein. Adding aluminum, a metal with greater electronic complexity, then tests the capability of the framework to describe more spectroscopically rich species and its facility and utility with multicomponent systems. The potential of this approach to serve as an active partner in the experimental search for new molecules is also described.

A. Alkali Metal Vapors

A series of spectra obtained under a variety of conditions with lithium vapor as the absorbant is displayed as Figure 1. The unresolved atomic resonance doublet ($2s \rightarrow 2p$) can be seen as the strong feature around 670 nm and the two optical molecular bands are the X $(1^1\Sigma_g^+) \rightarrow$ A $(1^1\Sigma_u^+)$ more broadly distributed around 670 nm and the X $\rightarrow$ B $(1^1\Pi_u)$ seen around 480 nm. The peak at 590 nm is the resonant line of contaminant sodium. The process of predicting all these features can be divided into the determination of the composite parameters required by the theoretical framework. Each of these is discussed in turn as models of increasing complexity are applied to a representative spectrum.

1. Lithium Atom State Energies and Oscillator Strengths

Accurate experimental sources for atomic state energies[14] and transition oscil-

---

[12] C.W. Larson, "The Spectroscopy of Hydrogen/Metal-Vapor Mixtures at High Temperatures and Pressures," *AL-TR-88-080*, Edwards AFB, CA, August 1990.

[13] For a briefer description see, C.W. Larson, M.E. Fajardo, P.G. Carrick, P.S. Erdman, W.C. Stwalley, J.D. Mills, and P.W. Langhoff, "Absorption and Emission Spectroscopy of High-Temperature Metal Vapors for Solar Thermal Propulsion," *JANNAF Propulsion Meeting*, Monterrey, CA, Nov. 1993.

[14] C.E. Moore, *Atomic Energy Levels*, Nat. Bur. Stand. Circ. 467, (U.S. G.P.O, Washington, D.C., 1949), Vol. I.

lator strengths[15] are used to provide the positions and intensities of the electronic transitions in atomic lithium.

2. Atomic Line Shape–Voigt Profile

In order to accurately account for the homogeneous and inhomogeneous broadening expected to be important in the gaseous samples of interest, a simple, symmetric peak shape which contains both Lorentzian and Gaussian components seems a reasonable first choice for the atomic transition lineshape. Thus, use is made of the energy-normalized Voigt profile,[16,17] the function which results from the convolution of Gaussian and Lorentzian distribution functions, as:

$$\phi_{IF}(E) = \int_{-\infty}^{+\infty} \left[\frac{1}{2\pi} \frac{\delta}{(E' - E_{IF})^2 + (\delta/2)^2}\right] \left[\frac{2\sqrt{\ln 2}}{\gamma\sqrt{\pi}} \, e^{-(4\ln 2)(E - E')^2/\gamma^2}\right] dE' \tag{24}$$

where δ is the Lorentzian width adequate for natural and collisional broadening and the Doppler and instrument broadening are represented by a composite Gaussian width, γ. For computational convenience this is calculable as the real part of the complementary error function of complex argument:

$$\phi_{IF}(E) = \frac{2\sqrt{\ln 2}}{\gamma\sqrt{\pi}} \mathrm{Re}\left\{\mathrm{cerfe}\left(\frac{\sqrt{\ln 2}}{\gamma}\left[2(E - E_{IF}) + i\,\delta\right]\right)\right\}. \tag{25}$$

For the resonant transition in lithium the natural width ($\approx 2 \times 10^{-4}$ cm^{-1})[18] is extremely small compared with that resulting from the other broadening processes. The instrumental width of 0.5 nm (8–30 cm^{-1} in the spectral region of interest and 11 cm^{-1} for the resonance transition)[19] is well characterized, as is that due to the Doppler broadening:[20]

$$\gamma_D = \frac{2E_{IF}}{c}\sqrt{\frac{2kT\ln 2}{m}} \approx 0.17 \text{ cm}^{-1}, \tag{26}$$

for an equilibrium distribution of absorbers of mass, m, with transition energy, E_{IF}, and at a temperature, T. Only the predominant Lorentzian component, the

15 W.L. Wiese, M.W. Smith, and B.M. Glennon, *Atomic Transition Probabilities*, Nat. Stand. Ref. Data Ser., Nat. Bur. Stand. Circ. 4, (U.S. G.P.O, Washington, D.C., 1966), Vol I.

16 G. Blendstrup, D. Bershader, and P.W. Langhoff, *J. AIAA*, **16**, 1106 (1978).

17 J.F. Kielkopf, *J. Opt. Soc. Am.*, **63**, 987 (1973).

18 A.C.G. Mitchell and M.W. Zemansky, *Resonance Radiation and Excited Atoms*, (Cambridge Univ. Press, London, 1971), pp. 96-97.

19 Unlike the physical widths this is fixed in wavelength rather than energy as the spectrometer disperses light on a scale linear in wavelength.

20 H.R. Griem, *Plasma Spectroscopy*, (McGraw-Hill, New York, 1964), pp. 101-102.

collisional or pressure broadening due to perturbation by neighboring bodies, is less well known. For typical gaseous samples the largest contributions to this component are linear in the concentrations of perturbers[21] and for atomic lithium in the present experiments significant terms exist for the strong, resonant self interaction between two alkali metal atoms and the weaker, nonbonding perturbation by the relatively more numerous rare-gas buffer atoms, as:

$$\delta_P^{Li} = C_{Li-Li}(\tfrac{N}{V})_{Li} + C_{Li-Rg}(\tfrac{N}{V})_{Rg}. \qquad (27)$$

The constant for the alkali/rare-gas interaction has been determined by repeated experiment to be approximately 2.2×10^{-20} cm^{-1}/cm^{-3}.[22] The value for the lithium self interaction is less well characterized with extrapolation from theory[23,24] giving a value of 1.6×10^{-17} cm^{-1}/cm^{-3} and a somewhat indirect experimental study[25] yielding 1.1×10^{-18} cm^{-1}/cm^{-3}. Theoretical modelling of the spectra in Figure 1 has managed to narrow the uncertainty associated with this parameter to $3-6 \times 10^{-18}$ cm^{-1}/cm^{-3} and gives total Lorentzian widths which fall in the range, $0.9 - 2.7$ cm^{-1}, for the differing thermodynamic conditions represented. Though it will be noted that the Gaussian width is several times larger, the more rapid exponential fall off of its profile leaves Lorentzian pressure broadening as the major component in the far-wing regions of the cross section which determine the width of the strongly saturated and broad transmission lines of Figure 1.

3. Model Absorption Due to Atoms

With the atomic parameters thus far described the intrinsic per atom absorption cross-section can be unambiguously calculated by equations (3) and (4). In equations (1) and (2) this can be combined with an atomic particle density (the calculation of which requires knowledge of some molecular parameters, and hence the discussion of which is deferred) and a path length (fixed to correspond to the experimental apparatus) to yield the absorption due to atoms alone. Figures 2 and 3 with typical and identical particle densities and temperatures of 1600K and 3000K, respectively, show the relative importance of higher atomic transitions. Ignorance of the broadening parameters associated with these transitions motivates the use of the resonant values throughout.

4. Calculation of Molecular State Energies

In order to predict both the positions of spectral transitions and the total number densities of each of the chemical species, the diatomic energy states must be calculated from the Born-Oppenheimer interaction energy curves. For diatomic lithium high quality experimental curves for the relatively isolated ground X

[21] E.L. Lewis, *Physics Reports*, **58**, 2, 1980.
[22] N. Allard and J. Kielkopf, *Rev. Mod. Phys.*, **54**, 1103 (1982).
[23] K. Niemax and G. Pichler, *J. Phys. B*, **8**, 179 (1975).
[24] B. Bussery and M. Aubert-Frëcon, *J. Chem. Phys.*, **82**, 3224 (1985).
[25] B. Ya'akobi, *J. Quant. Spectrosc. Radiat. Transfer*, **9**, 309 (1969).

($1^1\Sigma_g^+$) state[26,27,28] as well as the dipole-transition-accessible A ($1^1\Sigma_u^+$)[29,30,31] and B ($1^1\Pi_u$)[32] states are extended to the extremes of internuclear separation by smoothly attaching the results of calculations specially tailored for these regimes (X[33] and A and B both[34,35]) and making use of theoretically sound forms of extrapolation. These highly accurate hybrid potential energy curves[36] support bound states very near to dissociation (in all cases, to within approximately 0.3% of the total well depth). A single potential averaged over the small lambda-doubling splitting is used for the B state. With these three potential curves a modified version of a public computer program[37] allows numerical solution of equation (9) for the energies of a total of approximately eleven thousand rovibrational levels. Fractional populations of these levels are then calculable via the statistical mechanical expression of equation (11). For the high temperatures which exist in the experimental apparatus the consideration of many excited levels of the ground electronic state is necessary. At a typical temperature of 1600 K the total population of the v=18 manifold (dissociation occurs around v=40) is fully 1% of its value for the v=0 set of levels. Also, the peak in the rotational population distribution of the v=0 manifold occurs around J=30. Thus, in consideration of the $|\Delta J| \leq 1$ dipole selection rules, all bound eigenstates of all electronic states with rotational quantum number up to the dissociation of the ground electronic state (J = 123) are fully included.

5. Determination of Equilibrium Constants and Number Densities

Equation (2) for the optical absorption coefficient of a sample requires knowledge of the absolute particle density of each atom and molecule. Previously measured values[38] of the equilibrium vapor pressure above the condensed metal determine the total number density of lithium atoms due to both atomic and molecular species downstream in the observation zone. Then, the atomic and diatomic state

---

[26] M.M. Hessel and C.R. Vidal, *J. Chem. Phys.*, **70**, 4439 (1979).

[27] B. Barakat, R. Bacis, F. Carrot, S. Churassy, P. Crozet, F. Martin, and J. Verges, *Chem. Phys.*, **102**, 215 (1986).

[28] W.T. Zemke and W.C. Stwalley, *J. Phys. Chem.*, **97**, 2053 (1993).

[29] P. Kusch and M.M. Hessel, *J. Chem. Phys.*, **67**, 586 (1977).

[30] J. Verges, R. Bacis, B. Barakat, P. Carrot, S. Churassy, and P. Crozet, *Chem. Phys. Lett.*, **98**, 203 (1983).

[31] W.C. Stwalley, *unpublished.*

[32] M.M. Hessel and C.R. Vidal, *loc. cit.*

[33] W.T. Zemke and W.C. Stwalley, *loc. cit.*

[34] B. Bussery and M.Aubert-Frëcon, *loc. cit.*

[35] I. Schmidt-Mink, W. Müller, and W. Meyer, *Chem. Phys.*, **92**, 263 (1985).

[36] W.T. Zemke, K.K. Verma, T.H. Vu, and W.C. Stwalley, *J. Mol. Spectrosc.*, **85**, 150 (1981).

[37] W.T. Zemke and W.C. Stwalley, "Program Intensity," *Quantum Chemistry Program Exchange*, No. 477.

[38] A.G. Mozgovoi, I.I. Novikov, M.A. Pokrasin, and V.V. Roschupkin, *High Temp.-High Press.*, **19**, 425 (1987).

energies and mass conservation allow calculation of the particle densities of all species by equations (15)–(20). For the optimized model conditions corresponding to the spectra in Figure 1, particle densities of lithium atoms fall in the range 5.3×10^{13}–1.9×10^{18} /cm^3 and the ratio of diatoms to atoms ranges from 0.0000012 to 0.015. The atomic/diatomic equilibrium constants obtained in this way can be compared to those given directly by experiment[39] as in Figure 4. Although perhaps not readily apparent given the exponential vertical scale, the two sets of equilibrium constants differ by a factor of two at some of the lower temperatures of interest. Thus, at least for the present system, a statistical mechanical sum over essentially experimental state energies provides a measure of atom/diatom equilibrium superior to that from more direct measurement.

6. Determination of Transition Strengths

For diatomic lithium each of the three components of the combined molecular transition strength can be determined in turn. Contemporaneous with the calculation of the molecular state energies, numerical integration of equations (12) and (13) allows the relative intensity of state-to-state transitions to be determined to the two described levels of exactness given the transition dipole moment from electronic structure calculations[40] and the vibrational eigenfunctions. Also, different sets of London-Hönl factors for the X $\rightarrow$ A (of electronic symmetries $^1\Sigma \rightarrow ^1\Sigma$) and X $\rightarrow$ B ($^1\Sigma \rightarrow ^1\Pi$) manifolds are well known[41] and easily included. Finally, the overall electronic band oscillator strengths, $\bar{f}^{abs}_{X \rightarrow A} = 0.459$ and $\bar{f}^{abs}_{X \rightarrow B} = 0.958$, are provided by the potential curves and transition dipole moments parameterized to the equilibrium separation of the ground electronic state. These transition strengths and other information already described completely describe the total intensity of a molecular band at the rovibronic level (Eq. (7)). Succeeding approximations to attempt to accurately distribute this absorption intensity across the spectrum in appropriate lineshape functions will be described in the next few sections.

7. Vibronic Stick Spectrum

Before moving on to the most detailed case, the absorption cross section averaged over rotational degrees of freedom can be very economically calculated with the vibronic expression of equation (5). At the crudest level still consistent with a distributed electronic transition band, the cross section of each of the vibronic components can be represented by the height of a single stick. After selecting from the more complete rovibronic set of energies and Franck-Condon factors those of the $J'' = 0 \rightarrow J' = 0$ manifold to serve as effective values for the vibronic transitions and determining level populations by direct summation over the effectively singly degenerate levels (*c.f.* eqn. (9)), Figure 5 is obtained, in which the sticks

[39] A.N. Nesmeyanov, *Vapour Pressure of the Elements*, J.I. Carasso, Ed. and Transl., (Academic, New York, 1963), pp. 120-126, 456.

[40] L.B. Ratcliff, J.L. Fish, and D.D. Konowalow, *J. Mol. Spectrosc.*, **122**, 293 (1987).

[41] G. Herzberg, *Molecular Spectra and Molecular Structure: I. Spectra of Diatomic Molecules*, 2nd Ed., (Van Nostrand, New York, 1950), pp. 208-9.

are placed on an arbitrary inverted scale to mimic optically thin transmission and are superimposed on the corresponding experimental spectrum of Figure 1 (also displayed separately for future reference as Figure 6). It should perhaps be noted again that, as manifested by the complexity of the spectrum with transitions of significant magnitude occurring from several initial vibrational manifolds, there is significant thermal population of many vibronic levels above the lowest. Also, special mention should be made of both the close qualitative association which results from such a simple treatment and the ease with which it can be constructed–often without the need to perform any vibrational eigenfunction calculations or consider the rotational degrees of freedom in any way.[42] (In fact, Figure 5 was generated in this way, directly and early on, on the basis of published experimental results.[43,44])

8. Vibronic Spectrum with Realistic Lineshape

In order to create a model spectrum comparable to the experiment on an absolute scale, the stick vibronic strengths need only be broadened by an appropriate lineshape function and added to the atomic contribution. Deferring for the moment the question of the detailed characteristics of all the various contributions to the molecular lineshape, the predominance of the largest component, that due to instrumental broadening, can be qualitatively justified. Unlike the broad, saturated atomic doublet, molecular intensity is widely dispersed with many transition peaks carrying a tiny fraction of the total intensity and centered at a slightly different transition energy. Thus, in conjunction with the relative paucity of molecules, the transition lines show a less pronounced tendency to saturation, and, unlike the case with atomic widths, the process giving the largest absolute width may be expected to be the main determinant of molecular peakshape.

The manifold of $v'' = 0 \rightarrow v' = 0$ rovibronic transitions of the $X \rightarrow B$ band provides an illustration of the effective vibronic lineshape which results from these considerations. Since molecular transition widths for this system are not known, the approximate distribution of rovibronic intensities in a vibronic band can be illustrated by the use of sticks with length proportional to the relative strength of the level-to-level components. For the conditions corresponding to the experimental reference spectrum, this rotational analogue of the vibronic stick spectrum is shown as Figure 7. Also included in Figure 7 is the single broadened peakshape which results from convolving these strengths with the instrument function of width, 0.5 nm (approximately 21 cm^{-1} at this energy).[45] Here the closely spaced lines of this congested spectral region can be seen to produce an effective bandshape almost an

[42] It is simply mentioned that use of strength factors from some other, perhaps more thermally typical, rotational manifold had little effect upon the model spectrum. Further discussion relevant to this point can be found in section 9.

[43] P. Kusch and M.M. Hessel, *loc. cit.*

[44] M.M. Hessel and C.R. Vidal, *loc. cit.*

[45] Although unknown, analogy with the lithium atom suggests that the widths due to the other processes may be one or two orders of magnitude smaller than that due to instrumental broadening.

order of magnitude wider than the intrinsic width with which each component is actually broadened.[46] If a similar structure, the specific shape of which depends critically upon the relative energy spacings of upper and lower rovibronic levels, is calculated for the analogous manifold of the other electronic band, the widths at half maximum ($X \rightarrow A$: 215 cm^{-1}; $X \rightarrow B$: 156 cm^{-1}) can be used as constant effective peakwidths for all vibronic components of each band. Using an easily calculated Lorentzian peak shape for both the molecular and atomic components, the broadened vibronic spectrum, Figure 8, can be very rapidly determined. Its close correspondence to that measured (Figure 6) should be especially noted. As there is some uncertainty concerning the experimentally measured evaporator temperature, this has been adjusted to give most favorable agreement with experiment.

9. Rovibronic Spectrum

If the fuller, more resource-intensive treatment of equation (7) is employed and all molecular degrees of freedom are included in both the transition energies and the transition-dipole-dependent strengths, an even more realistic spectrum, Figure 9, is obtained. The close association with experiment is seen in Figure 10 where both are displayed together. Although some effects due to rotation are in evidence, as will be demonstrated subsequently, the broad instrumental function prohibits resolution of individual rovibronic lines. Using optimized evaporator temperatures but experimental observation temperatures, a complete set of five model spectra corresponding to the experimental group of Figure 1 can be modelled. These are displayed together in Figure 11.

At this juncture the effects of approximations designed to reduce the amount of information or resources required to generate such spectra might be profitably investigated. Although the distribution of vibronic intensity across the spectrum in separate peaks of rotationally dependent transition energy clearly results in a qualitatively different spectrum, the rotational dependence of the intrinsic strengths of these state-to-state peaks was found to be rather small. By applying the hybrid approach described in section IB2, spectra in which all rovibronic transitions are given their corresponding intrinsic strength in the $J'' = 0 \rightarrow J' = 0$ manifold are virtually identical to those modelled with full rotational dependence. The degree of similarity is approximately the same if higher, more thermally typical, values of $J'' = J'$ are used. Thus, at least for these two electronic bands, the changes in the expectation value of the transition dipole moment with commensurate adjustment of initial and final rotational state seem to either be small or effectively compensate. This simplification dramatically reduces the time and storage required to generate and incorporate the transition strengths, and thus should be aggressively pursued in modelling the spectra of other molecules.

---

[46] The additional effective broadening which can result from molecular congestion can be quite important for the quantitative optical properties of a sample even when measurement with a low-resolution instrument is not at issue. The implications of this circumstance for spectral modelling is discussed in more detail in the following section.

Also, the effects of the Franck-Condon Approximation can be more precisely gauged. In this case spectra which result from use of Franck-Condon strengths are simply indistinguishable from their more exact counterparts on the scale used to display them. This seems justified by the mild variation of the transition dipole moment with internuclear separation for the two transitions. These functions are displayed in Figures 12 and 13 along with the ground potential energy curve which governs the distribution of the average internuclear separation of the initial states. Systems for which the Franck-Condon Approximation is adequate have the advantage of not requiring a theoretically determined transition dipole moment for the accurate modelling of their spectroscopy.

10. Lineshape–Further Issues

The present computational framework should, in principle, allow unprecedented investigations into the fundamental processes governing the lineshape of both atomic and molecular transitions. Beyond a determination of the magnitude of the various components of the width of the atomic resonance line, the modelling described here should allow a characterization of the asymmetry due to subtle perturbative effects in the collisional self-broadening. For broad, saturated lines this asymmetry can have a significant effect upon the optical properties of the vapor and although it has been observed and measured in the other alkali metals,[47,48,49] the unique presence of the overlapping molecular band in lithium prohibits its direct measurement at the high particle densities necessary. By subtracting the modelled molecular component from the experimental spectrum, the asymmetric absorption due to the atoms alone could be characterized. Also, preliminary results indicate that hydrogen added to the reaction stream may increase the atomic linewidth as formation of molecules in the dynamic chemical equilibrium provides another pathway for the decay of excited atomic states. One can easily imagine that changes in width due to other nonradiative processes might be measurable as well. More accurate accounting for experimental baseline drift and careful comparison with model spectra should allow quantification of these effects, and may lead to further refinement of the theoretical perspectives commonly used to explain them.

Progress may also be possible in defining the values, or at least determining the implications of possible values, of the totally unknown molecular widths. In particular, higher resolution measurements needed to attempt to resolve individual molecular lines can be directed and motivated by extensive modelling at a whole series of prospective resolutions and intrinsic linewidths. As a single example consider an expansion in scale of a small portion of the $X \rightarrow B$ molecular absorption. In Figure 14 the low-resolution experimental spectrum around the $v'' = 0 \rightarrow v' = 0$ band head without individually resolved lines is plotted with a model spectrum in which the linewidth is limited only by a narrower intrinsic width chosen for illustration

[47] K. Niemax and G. Pichler, *J. Phys. B*, **7**, 1204 (1974).
[48] K. Niemax and G. Pichler, *J. Phys. B*, **7**, 2355 (1974).
[49] K. Niemax and G. Pichler, *J. Phys. B*, **8**, 179 (1975).

from the broad range suggested by analogy with the lithium atom.

This type of procedure can be used not only to justify the gross structure of the low-resolution spectrum and predict and motivate high-resolution experiments designed to measure the intrinsic physical structure of molecular bands, but can also help to determine how the fraction of optical radiation actually removed by a sample in a particular wavelength range relates to the same value modelled and measured at finite resolution. For example, a sample with separated, narrow, highly saturated lines would absorb light much differently than would be modelled or measured upon broadening with the convolution function of a low resolution instrument. This might be especially important in energy exchange between samples with highly structured optical spectra. Conversely, a series of physical lines relatively narrow, but highly congested so as to yield a collective bandshape much broader than their individual intrinsic widths, might not present such a problem.[50] In this way, what might seem to be an esoteric property of a medium has the potential to strongly influence the bulk energy and optical-transfer properties and researchers seeking to use model spectra in the design of practical systems ignore it to their peril.

11. Other Capabilities

By superimposing or subtracting model and experimental spectra, all sorts of detailed comparisons and characterizations are possible. The single example of a diatomic lithium triplet absorption band ($1^3\Sigma_u^+ \rightarrow 1^3\Pi_g$) which contains both bound-bound and bound-free components is presented here. In Figure 15 a portion of a model spectrum without contributions from these states is displayed on an expanded scale with the same portion of the corresponding experimental spectrum. The absence of the triplet feature in the model is also apparent by comparing the spectra in Figure 11 with their experimental counterparts in Figure 1. Although this absorption band has been previously observed,[52,53] it should be clear how this general technique could be of use in identifying novel features in the spectra of known molecules or even transitions of previously unobserved molecules. By subtraction new spectral features might even be extracted from the more intense background of a known, modelled interferent. The ongoing attempt to use this approach to identify chemical specie is described in section B.[54]

---

50 The resonant refractive index measured at high resolution might provide the most convenient means of distinguishing between these two circumstances because of its extreme sensitivity to the overall strength and width of separated absorption peaks. The linear dependence of the signal strength upon particle number density might even provide a sensitive diagnostic of the thermodynamic conditions in locally equilibrated flowing gases.[51]

51 G. Blendstrup, B. Bershader, and P.W. Langhoff, *op. cit.*.

52 D. Vezǎ, S. Miloševič, and G. Pichler, *Chem. Phys. Lett.*, **93**, 401 (1982).

53 F. Martin, R. Bacis, J. Vergès, C. Linton, G. Bujin, C.H. Cheng, and E. Stad, *Spectrochim. Acta*, **44A**, 1369 (1988).

54 Although it cannot be cited as a positive success, it should perhaps be mentioned that a model analysis of the already characterized $X\,(1^1\Sigma_g^+) \rightarrow C\,(1^1\Pi_u)$ transition

12. Sodium Spectra

The present theoretical and computational framework has also been applied to modelling spectra of the sodium system. As the thermodynamic and chemical conditions of the experiments are somewhat less well known, no results are displayed here. Nonetheless, it should be noted that the spectra of this isoelectronic system are qualitatively similar to those of lithium and that the comments relative to the validity of the Franck-Condon Approximation and the rotational independence of transition strengths likewise obtain.

B. The Mixed Aluminum/Lithium System

Of the atomic and diatomic species, Li, Al, Li_2, Al_2, AlLi, which exist in an equilibrium mixture of lithium and aluminum, the heteronuclear diatomic has apparently never before been observed. As the weak transitions of diatomic aluminum and the strong signals due to atomic and diatomic lithium occur in the same region of the spectrum in which theoretical calculations predict absorption by AlLi, this two-metal system would seem to provide a good next step in testing the feasibility of extracting the experimental spectrum of novel molecules from a known background as well as further characterizing the accuracy of the various approximations expedient in the model. Also, a significant bound-free absorption in diatomic aluminum allows extension of the framework to transitions of different character. Even before modelling the absorption due to AlLi, theory can be of aid in preparing for the experiments in three areas: design of thermodynamic conditions expected to maximize production of the molecule of interest, prediction of the weak, potentially interfering optical bands of diatomic aluminum, and description of the expected total spectral background upon which any AlLi signal would have to be measured. Each of these is explained in turn with a view toward determining thermodynamic conditions in which the desired signal is maximized and the interference is minimized.

1. Particle Densities of All Species and Molecular Energy Levels

In addition to the atomic and molecular constants of the lithium species, determination of the thermodynamic parameters of an equilibrium mixture of lithium and aluminum requires the temperature-dependent vapor pressure above condensed aluminum,[55] the energy levels of atomic aluminum,[56] and the energies and degeneracies of at least the lowest, thermally significant states of Al_2 and AlLi.

For diatomic aluminum the rovibronic state information is taken from energy

---

of lithium was able to contra-indicate assignment of a very weak series of lines in the appropriate spectral region to this transition.

[55] A.N. Nesmeyanov, *op. cit.*, pp. 232-237, 459.

[56] C.E. Moore, *op. cit.*

expansions obtained from experiment[57,58,59] or provided by the eigenvalues (eqns. (9) and (10)) of the molecular potential curves given by extensive *ab initio* electronic structure calculations.[60] For states involved in the dipole spectroscopy, the theoretical energy values (sometimes shifted so that the dissociative limits of upper states correspond with experimental atomic transition energies) are used exclusively. The energy splitting due to interactions between nuclear rotation and electronic angular momenta are neglected in all but the lowest potential curve (in which case these effects are represented by a constant value obtained from the lowest experimental levels). In this way, seven electronic state manifolds and around 8×10^4 states with rotational quantum number up to 200 are included in the calculation of the partition function of diatomic aluminum. For AlLi preliminary electronic structure calculations[61] provide simple energy expansions for the two thermally significant electronic states.

With the energies and degeneracies of all atomic and diatomic states the populations of all five species can be determined via equations (15)–(20) in a manner only algebraically more complicated than that used for the simple one-component, two-species lithium system. As a single illustration of the parameter space thus defined, Figure 16 shows the dependence of the five particle densities upon lithium-evaporator temperature with fixed aluminum-evaporator and observation-zone temperatures.

2. Diatomic Aluminum Spectroscopy

In contrast to diatomic lithium two electronic states of the aluminum molecule are predominantly populated at the high temperatures of experimental interest. For the ground X ($1^3\Pi_u$) state there are optical, dipole transitions to the mostly repulsive $1^3\Pi_g$ state (referred to hereafter as R). Similarly the bound A ($1^3\Sigma_g^-$) state with energy minimum a mere 220 cm^{-1} above that of the ground state can be similarly coupled to the bound B ($1^3\Sigma_u^-$) state. As the strongest transitions out of both of these states involve absorption in the ultraviolet, it is not surprising that the lower-energy transitions are extremely weak. This is quantified in the overall band oscillator strengths derived from *ab initio* transition dipole moments:[62] $\bar{f}^{abs}_{X\rightarrow R} = 0.027$ and $\bar{f}^{abs}_{A\rightarrow B} = 0.009$. Combined with the relative paucity of molecules at the relevant temperatures, this leads to the expectation that Al_2 will be only a weak

57 Z. Fu, G.W. Lemire, G.A. Bishea, and M.D. Morse, *J. Chem. Phys.*, **93**, 430 (1990).

58 M.F. Cai, C.C. Carter, T.A. Miller, and V.E. Bondybey, *Chem. Phys.*, **155**, 155 (1991).

59 Although experimental studies have been conducted on some of the electronic states of Al_2, the energy expansions derived from them cannot accurately account for the high vibrational levels necessary in a complete treatment of the spectroscopy. In fact, for the ground manifold of states, differences between experiment and theory are within experimental error.

60 S.R. Langhoff and C.W. Bauschlicher, *J. Chem. Phys.*, **92**, 1879 (1990).

61 M.E. Rosenkrantz, *in progress.*

62 S.R. Langhoff and C.W. Bauschlicher, *loc. cit.*

interferent in the search for AlLi at optical frequencies. This minor contribution can nonetheless be modelled in the present framework.

a. Vibronic Stick Spectra and the Bound-Bound Transition

Frank-Condon factors and transition dipole matrix elements for the A → B transition are provided by the initial- and final-state Born-Oppenheimer potential curves and the transition dipole moment. Using the transition energies and strengths of the rotationless rovibronic states, the vibronic stick spectra of Figures 17 and 18 are obtained for one set of experimentally accessible thermodynamic conditions and with arbitrary but identical vertical scaling. The Franck-Condon strengths used for Figure 17 are replaced by their more exact counterparts to produce the spectrum of Figure 18. For this transition band the Franck-Condon Approximation is clearly not adequate to accurately account for the absorption profile. This can be justified from the transition dipole moment and the initial state potential curve displayed in Figure 19. It should come as little surprise that a transition dipole which varies rapidly from a small value on either side of the initial state equilibrium separation is not well represented by an average value independent of state. That a similar situation exists for the X → R transition can be seen in Figure 20. Thus, the strength factors derived from transition dipole matrix elements will be used exclusively in the modelling which follows.

b. Broadened Vibronic Spectra and the Bound-Bound Transition

If it is again assumed that the rotational structure of a rovibronic manifold will be obscured by the large instrumental width,[63] an effective vibronic width can be obtained from a broadened stick spectrum analogous to Figure 7. When this 88 cm^{-1} breadth is transferred to a Lorentzian profile centered at the rotationless transition energies, the broadened absolute absorption, Figure 21, can be determined. The vertical scale and the extreme weakness of this transition are especially to be noted.

c. Including the Bound-Free Transition with Vibronic Resolution

For the bound-free X → R transition further approximations to the continuum analogues of the strength factors, equations (12) and (13), are used in this study. The final state in a transition to a repulsive electronic curve is described by a non-square-integrable, continuum wave function with limiting sine-wave behaviour far from the interaction region and average probability density greatest near the classical turning point. To a first approximation it is common to represent this wave function by a delta function at the turning point and to assume that the effects of the rest of the oscillatory wave function effectively cancel in the strength factor integral. Although conceptually rather crude, this procedure which has been

[63] Experimental values for the predominant linewidths in atomic and diatomic aluminum are nonexistent. However, even if the intrinsic widths are two orders of magnitude higher than those expected for lithium, this assumption still holds.

referred to as the reflection approximation[64] has been found to yield surprisingly accurate results and leads to strength factors of the form:

$$\chi^{\mu}_{v_i J_i, J_f}(E) = \frac{|\vec{\mu}(R_{T(E)})|^2}{|\vec{\mu}(R_{e,i})|^2} \frac{|\phi_{v_i J_i}(R_{T(E)})|^2}{\left.\frac{dE_f}{dR}\right|_{R=R_T(E)}} \qquad (28)$$

where the dependence on the transition energy is expressed parametrically in $R_{T(E)}$, the internuclear separation at which a point on the upper state curve, $E_f(R)$, lies exactly E above the initial state energy, and the derivative of the upper state energy with respect to internuclear separation results from normalization of the continuum wave functions on the energy scale. If these continually varying strengths are combined with the other factors of equation (6) and the angular momentum splittings in the ground electronic state are neglected, the total vibronic absorption due to both bound-bound and bound-free processes in diatomic aluminum, Figure 22, can be determined.[65] For this system the importance of the oft-neglected continuum transitions in accounting for the quantitative molecular absorption can be clearly seen.

d. Rovibronic Treatment of the Bound-Bound Component

Modelling the rotational structure of the spectrum of the aluminum molecule is made possible or more tractable by various simplifying assumptions. The lack of any firm values for the broadening coefficients for collisional interaction with all other species motivates the hope that at least the qualitative nature and shape of the bound-bound electronic band can be illucidated by using those in the middle of the range thought to be possible for diatomic lithium. Further, if all electronic and nuclear angular momentum interactions were considered strictly, twelve transition branches would result with the relative strength and separation of each depending upon the degree of the coupling. By neglecting the smallest splittings and weakest bands, the total preserved intensity can be grouped into two predominant bands with effective Hönl-London-type factors.[66] Even with these restrictions

---

[64] G. Herzberg, *op. cit.*, pp. 387-394.

[65] The jitter seen in the continuum contribution is due to the coarseness in the sampling of the strength factor required by storage constraints. For bound-bound processes the present framework allows all transitions to be approximately but accurately described by only two numbers, an intensity and a peak location, with the wavelength dependence of the intensity distribution of all peaks provided by a common lineshape factor. For bound-free processes the strengths themselves take on a nonseparable shape dependence and so this economy is not possible. The magnitude of the errors resulting from this difficulty is thought to be on the order of or smaller than that resulting from use of the reflection approximation. Thus, before attempting the bound-free rovibronic problem, seeking a wholly different approach which overcomes both limitations may provide the greatest promise. In any case different methods of calculating bound-free matrix elements should be understood to be fully consistent with the methodology of the present framework.

[66] G. Herzberg, *op. cit.*, pp. 208-209, 218-237, 245-251.

around 1.8×10^6 transitions must be considered. Finally, motivated by the savings allowed with the lithium molecule, the hybrid treatment is employed in which each of the rovibronic transitions is given its corresponding strength in the $J'' = J' = 0$ manifold. The distinctive shape, if not the strength, of the resulting spectrum, Figure 23, might make it easily recognizable in a stronger, but relatively featureless, interfering background.

In light of the weakness of the two aluminum bands and the current problem sampling the bound-free transition strength, valuable resources were not expended in an investigation of the effects of rotation upon the bound-bound transition strengths and the broad bound-free absorption, although these circumstances are equally well treated by the computational framework.

3. Background for Detection of AlLi

By combining the particle densities of all atoms and diatoms and the spectroscopy of dialuminum and the two lithium species with the measured aluminum atomic strengths[67] and some atomic aluminum linewidths chosen in analogy with the lithium atom, it is possible to model that portion of the absorption by an equilibrium aluminum/lithium mixture which is due to all monatomic and diatomic species except AlLi. To emphasize the relative weakness of absorption by Al_2 and to illustrate the breadth of the potentially interfering atomic-lithium shoulder, a single such spectrum is shown on two different intensity scales in Figures 24 and 25. Here the only new feature is the closely spaced $3p \rightarrow 4s$ resonance doublet of atomic aluminum around 395 nm.[68] Making use of plots of this type, the optimization of conditions expected to maximize the production of the unknown molecule can be modulated by the need to reduce the strength of absorbing contaminants. Thus, even before modelling the spectrum of the species of interest, the theoretical framework proves to be valuable in yet another way by helping to constrain labor-intensive searches over the experimental parameters.

4. Future Prediction of the Aluminum Lithium Spectrum

Very extensive calculations of the Born-Oppenheimer potential energy curves and electronic transition dipole moments of AlLi are currently underway[69] and when completed will allow unambiguous calculation of the absolute absorption due to AlLi. Preliminary results indicate that a particularly strong transition may be found around 650 nm (*c.f.* Figures 24 and 25). In all likelyhood a modelling framework which allows the subtraction of the spectra of strongly absorbing contaminants will be necessary to isolate any absorption due to the new molecule. After the solution of materials problems which stand in the way of containing and evaporating both elements in a controlled manner, measured spectra of the aluminum-lithium system

---

[67] W.L. Wiese, M.W. Smith, and B.M. Glennon, *op. cit.*

[68] In preliminary work with aluminum by itself in the Plasma Spectroscopy Cell, a weak but discernable doublet has been observed in this region.

[69] M.E. Rosenkrantz, *in progress.*

should be available for more exacting comparison between the present theoretical framework and experiment and the limitations imposed by necessary and convenient model approximations may be more clearly determined.

IV. Conclusions

From the modelling of particle densities to interpreting and predicting the final results of measured spectra, the present theoretical framework can be a valuable partner in spectroscopic studies of known and unknown chemical species existent under known equilibrium conditions. In particular, spectral modelling can help unite *ab initio* molecular structure calculations with experimental investigations by illustrating the results of the theory in a form directly comparable to what can be measured. Successes in the interpretation of the relatively well known atomic and diatomic spectroscopy of the alkali metals have been presented along with means of further investigating the nature and magnitude of the various line-broadening processes which are treated rather simply and empirically here but are critical to an accurate accounting of the bulk thermal and radiative transport properties of extended samples. In addition, the tested framework has been applied to more complicated and even wholly unknown systems in an effort both to concretely aid current experiments and to further verify the approach. The applicability of the Franck-Condon Approximation has been found to depend critically and predictably upon the transition moment between initial and final states; other simplifying approximations have been less satisfactorily justified. An extension of the modelling of the absolute magnitude of the optical absorption to include emission and the refractive index have also been outlined. These, along with some accounting of the effects of anisotropy and the finite extent of real samples, should allow more realistic modelling of absorption in prospective energy conversion devices and may play a role in the development of additional applications. Continuing close association with spectroscopic investigations using the Plasma Spectroscopy Cell and the extensive comparison of theory and experiment which this allows will be critical in validating and refining the present theoretical framework and in further evaluating the promise of close cooperation between these complementary approaches.

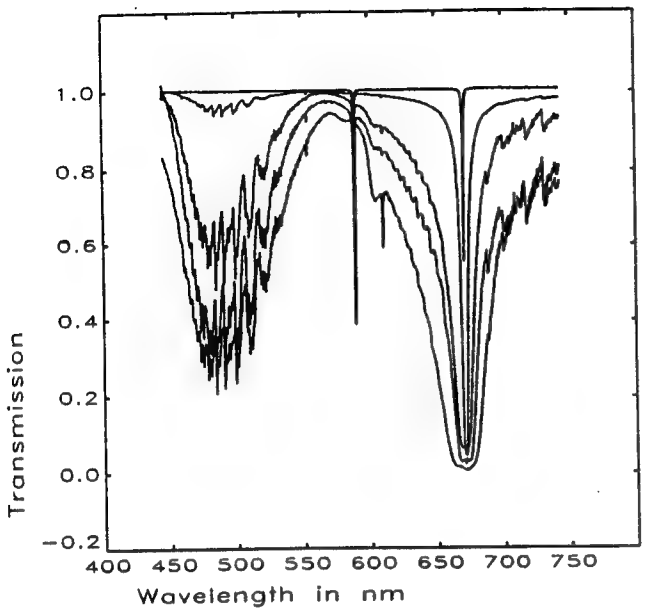

Figure 1—Absorption spectra measured with the lithium evaporator and observation zone temperatures in the ranges, $T_{evap} = 970-1390K$ and $T_{obs} = 1580-2033K$, and a total pressure of 1 atm.

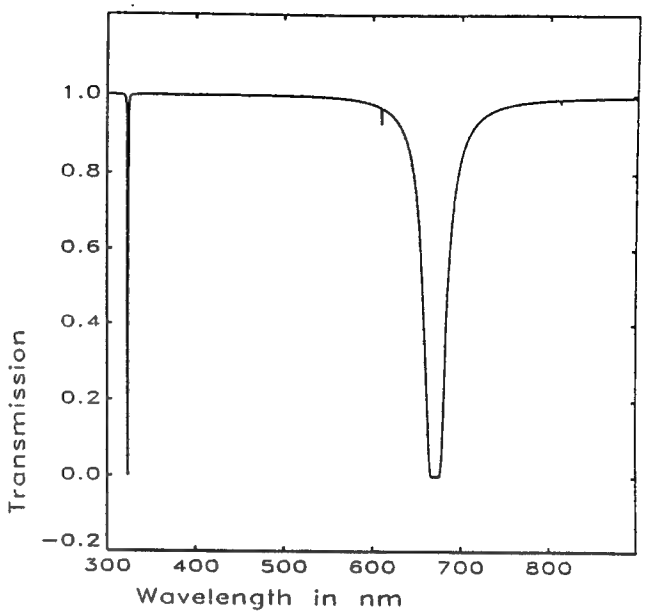

Figure 2—Model absorption by lithium atoms at a temperature of 1600K with number density, $7.9x10^{17}/cm^3$, predominant widths of each type, $\delta_{press} = 2.45\ cm^{-1}$ and $\gamma_{instr} = 0.5$ nm, and pathlength, $\Delta x = 3.5$ mm.

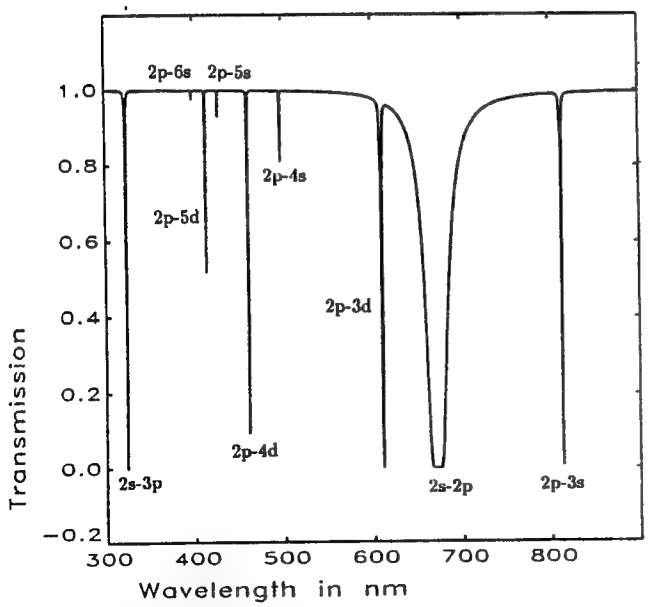

Figure 3—Model atomic absorption of a 3000K sample of lithium with number density and predominant widths identical to those of Figure 2.

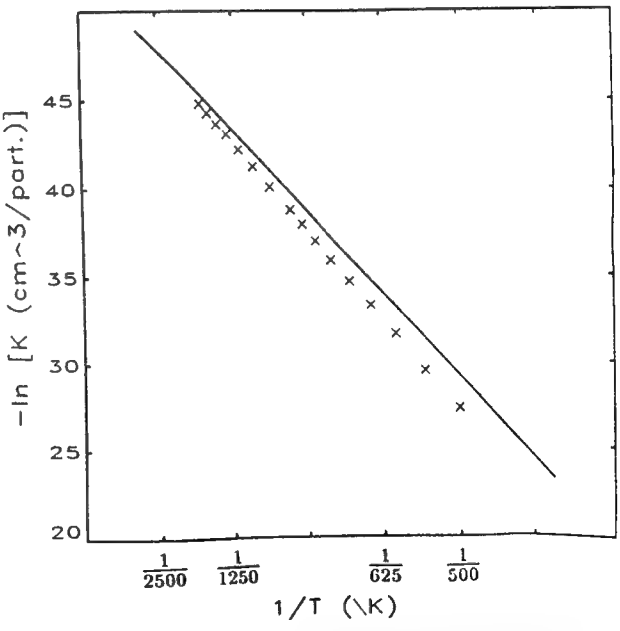

Figure 4—The temperature variation of the lithium atom/diatom equilibrium constant (defined in eqn. (17)). The line results from a statistical mechanical sum over experimental level energies and the discrete points are those reported in reference 39.

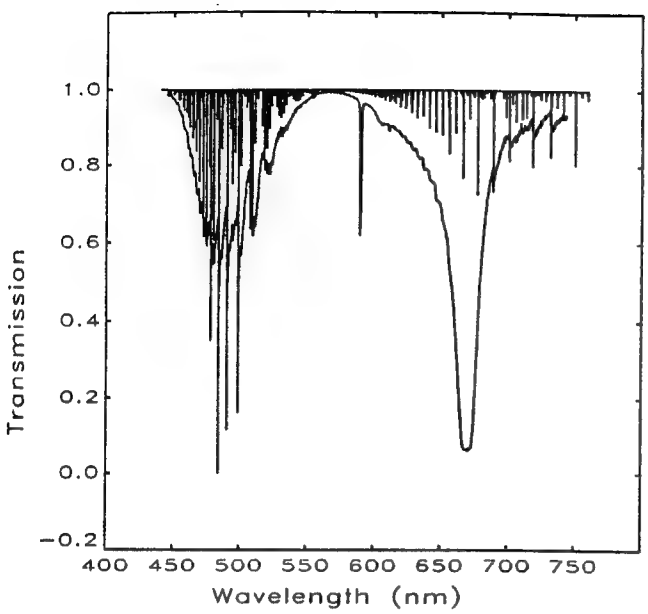

Figure 5—Vibronic stick spectrum for diatomic lithium alone, displayed with the corresponding experimental spectrum (also displayed as Figure 6) which includes an atomic component. The model observation temperature is the same as that measured experimentally.

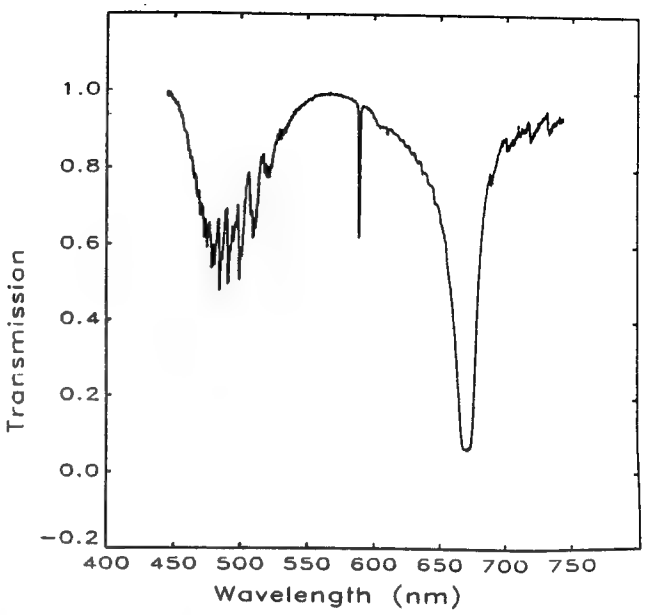

Figure 6—Reference experimental absorption spectrum displayed as the middle spectrum of Figure 1 with T_{evap} = 1334K and T_{obs} = 1703K.

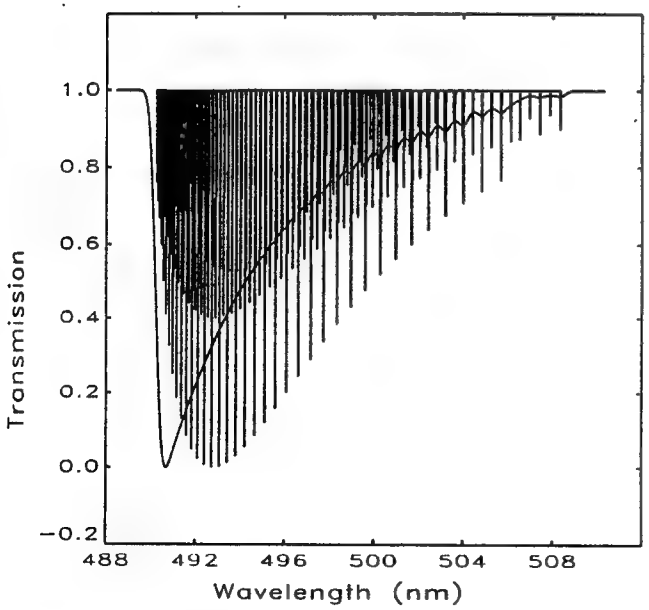

Figure 7—Stick spectrum representing the rotational structure of the $v'' = 0 \rightarrow v' = 0$ vibronic band of the $X \rightarrow B$ manifold of Li_2 displayed on an arbitrary scale with the distribution obtained with experimental broadening (0.5 nm).

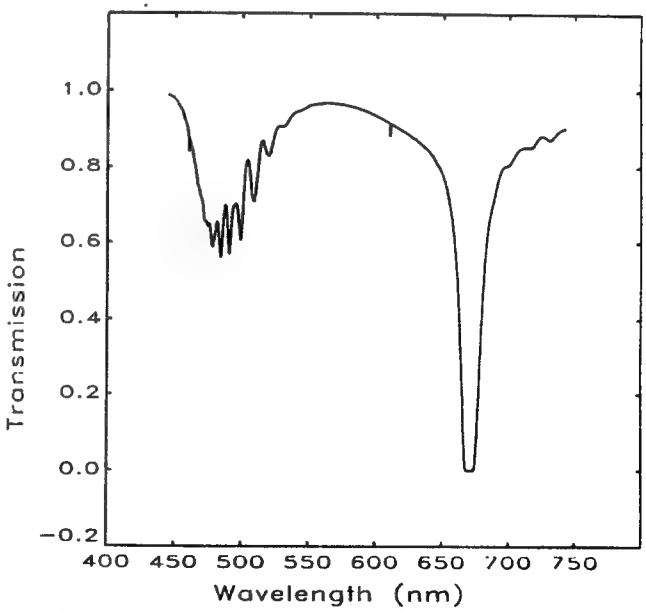

Figure 8—Broadened vibronic spectrum for an equilibrium mixture of atomic and diatomic lithium. T_{evap} = 1365K and T_{obs} = 1703K. Predominant atomic Lorentzian width: $\delta_{press} = 1.33\ cm^{-1}$ and molecular Lorentzian widths: $\delta_{vib}^{X \rightarrow A} = 215\ cm^{-1}$ and $\delta_{vib}^{X \rightarrow B} = 156\ cm^{-1}$.

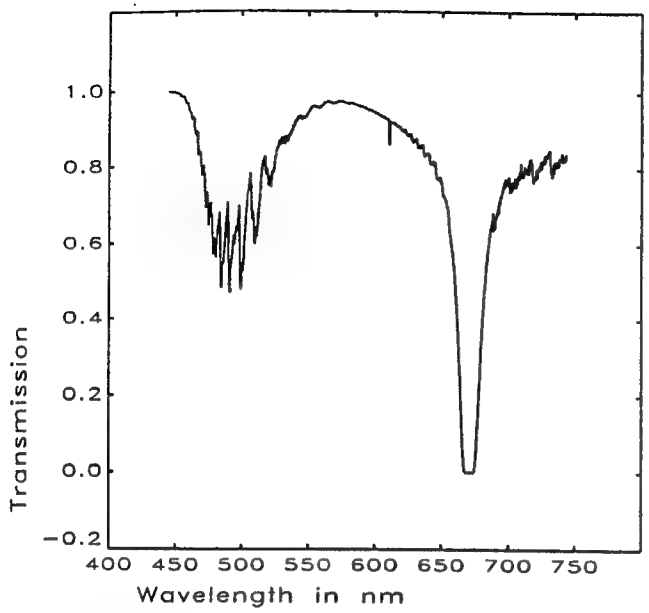

Figure 9—Rovibronic model spectrum with full rotational dependence included in both transition energies and strengths. T_{evap} = 1365K and T_{obs} = 1703K. Atomic widths are as in Figure 8 and the other predominant widths are, Gaussian: γ_{inst} = 0.5 nm and molecular Lorentzian: $\delta_{press} = 1.0\ cm^{-1}$.

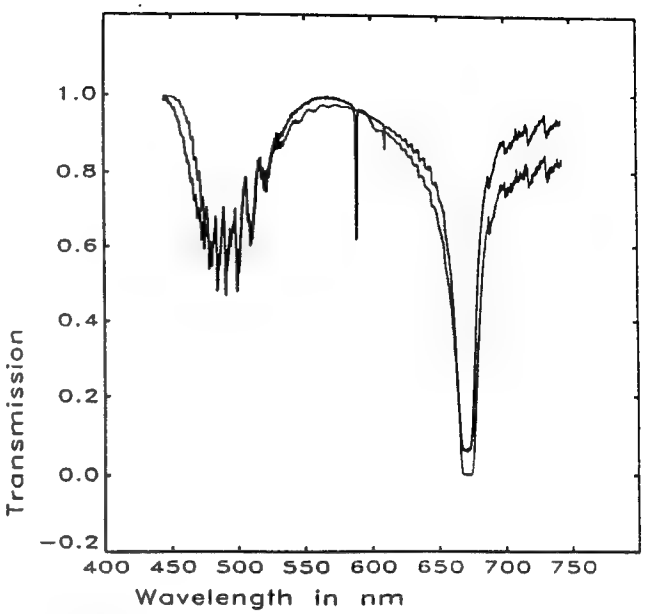

Figure 10—The optimal rovibronic model of Figure 9 (distinguishable by the absence of contaminant sodium around 590 nm) displayed with its experimental counterpart (Figure 6).

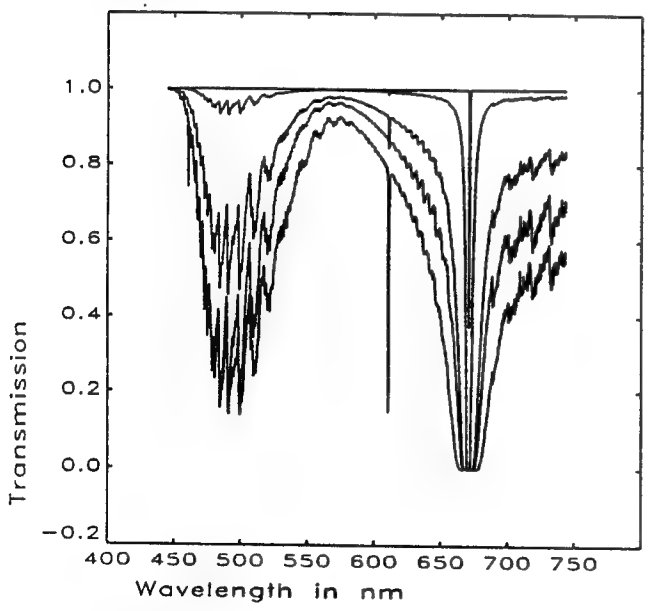

Figure 11—Optimal model rovibronic spectra corresponding to those displayed in Figure 1. Evaporator temperatures fall in the range, T_{evap} = 805 − 1510K, observation temperatures are those measured experimentally, instrumental widths and Lorentzian molecular widths are as in Figure 9, and atomic Lorentzian widths fall in the range, $\delta_{press} = 0.10 - 2.01\ cm^{-1}$.

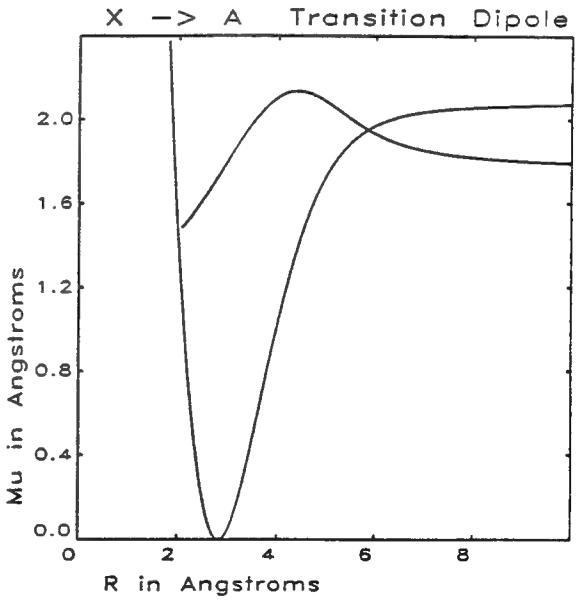

Figure 12—Born-Oppenheimer electronic transition dipole moment for the X → A transition. On a different (unlabeled) vertical scale (but identical horizontal scale) can be seen the ground state potential energy curve (depth, approximately 8500 cm^{-1}).

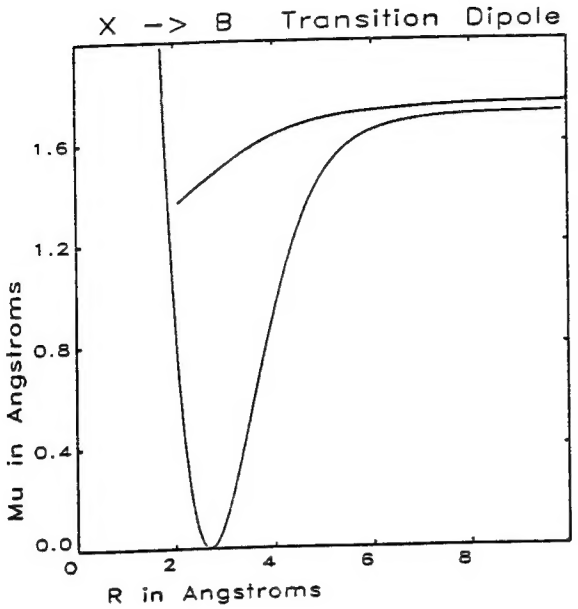

Figure 13—Transition dipole and ground state curve for the X → B transition.

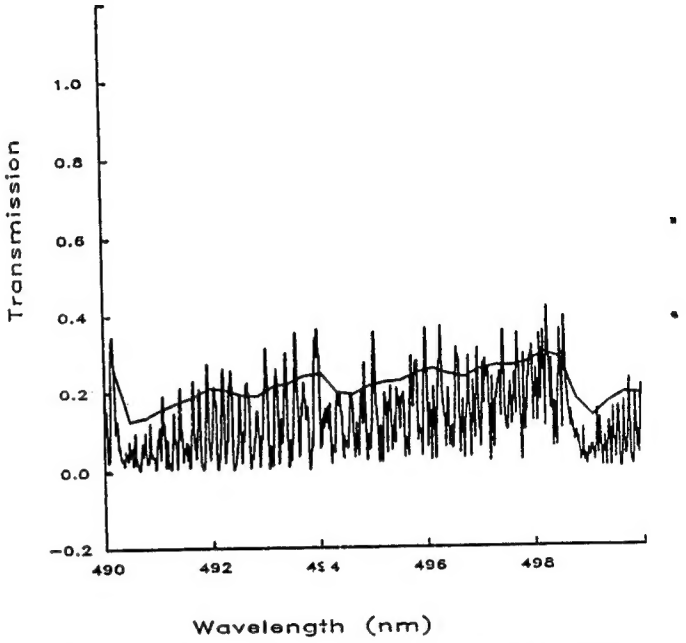

Figure 14—Low-resolution (γ_{instr} = 0.5 nm) experiment and high-resolution ($\gamma_{instr} \approx 0$) model spectrum on an expanded wavelength scale. The band head for the $v'' = 0 \rightarrow v' = 0$ manifold lies around 490.5 nm. Predominant molecular widths: δ_{press} = 1.0 cm^{-1} and γ_{dopl} = 0.132 cm^{-1}.

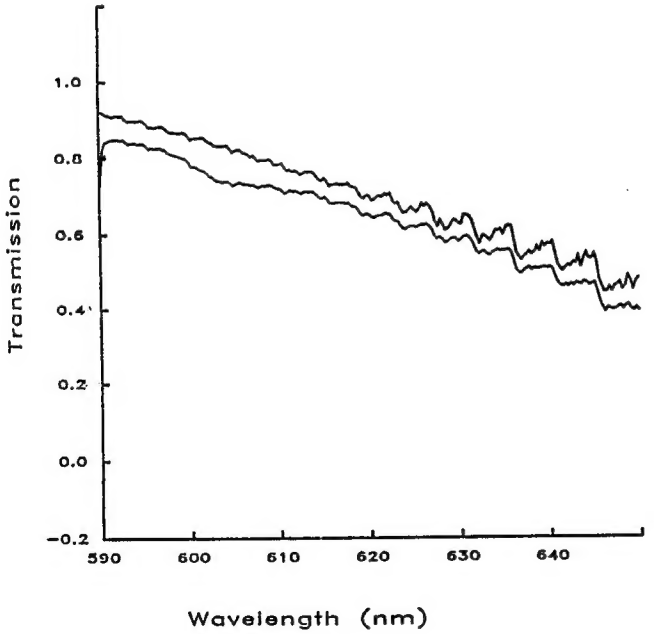

Figure 15—Model and corresponding experimental spectrum in the region of a triplet absorption. The model (top) lacks contributions from the ($1^3\Sigma_u^+ \rightarrow 1^3\Pi_g$) transition observed around 600-610 nm.

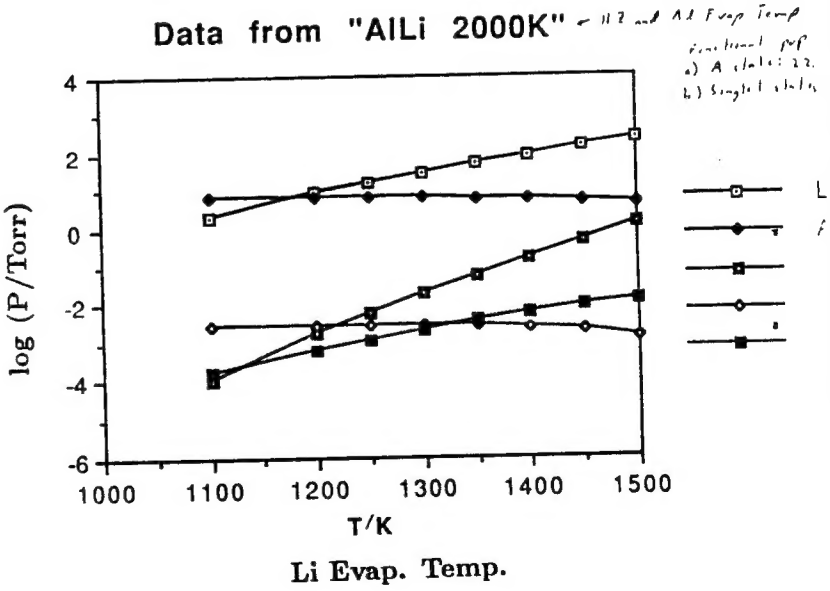

Figure 16—Dependence of the partial pressures of the species in the observation zone upon lithium evaporator temperature with aluminum evaporator and observation zone temperatures fixed to 2000K.

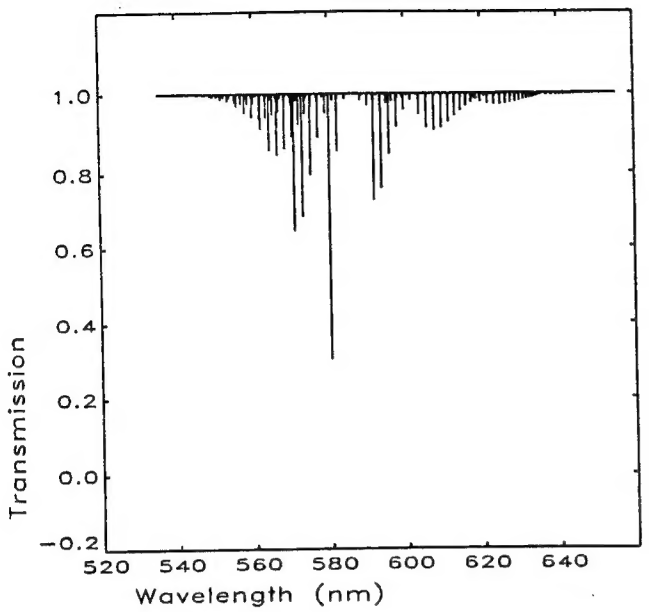

Figure 17—Franck-Condon vibronic stick spectrum for the bound-bound A → B transition of diatomic aluminum at $T_{obs} = 2100K$.

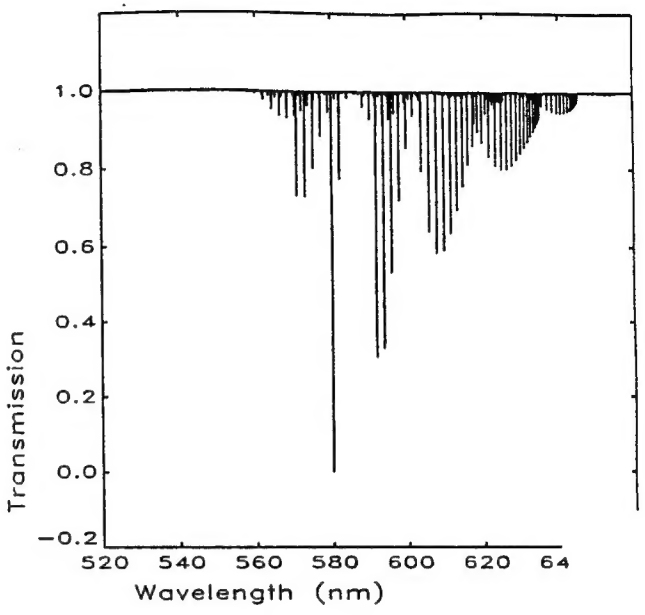

Figure 18—Diatomic aluminum vibronic stick spectrum incorporating strengths constructed from the transition dipole matrix elements and with $T_{obs} = 2100K$.

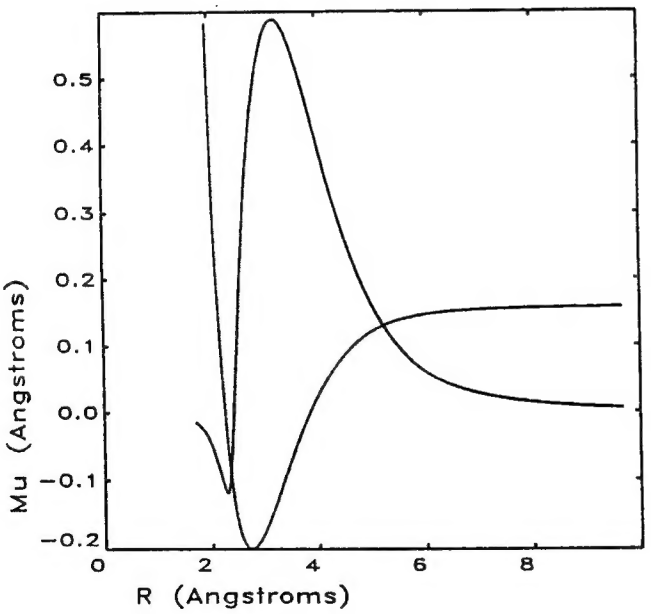

Figure 19—Electronic transition dipole for the bound-bound A → B transition in diatomic aluminum on the same horizontal scale as the initial-state potential energy curve. The depth of the initial state is approximately 11000 cm^{-1}.

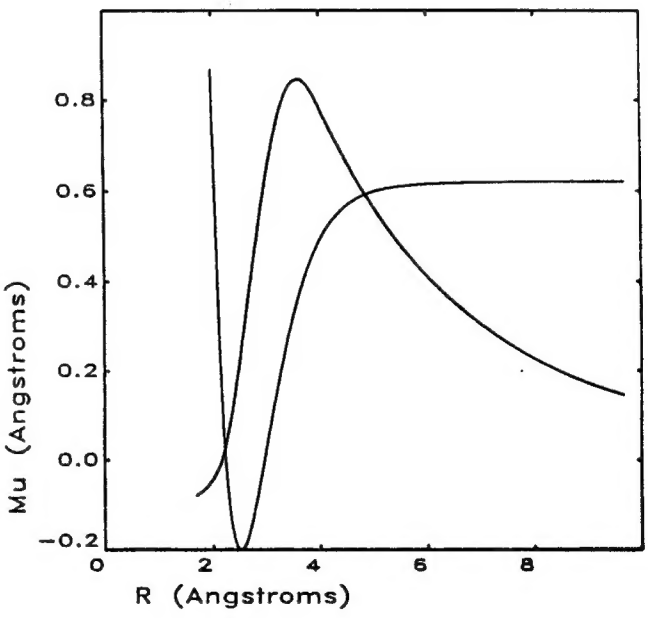

Figure 20—Transition dipole and initial state for the bound-free X → R transition. Here, the ground electronic state is also bound by approximately 11000 cm^{-1}.

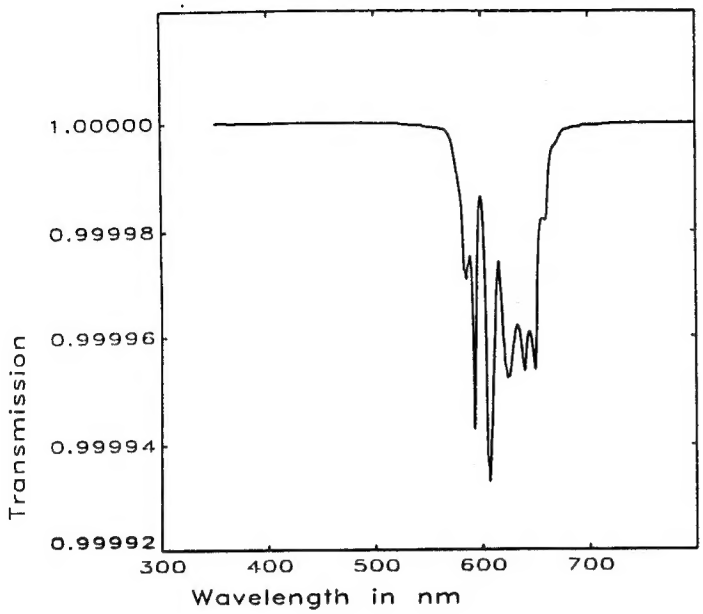

Figure 21—Broadened vibronic model of the bound-bound A → B transition in diatomic aluminum using strengths from transition dipole matrix elements. Here, $T_{evap}^{Al} = T_{obs} = 2100K$ and the only operant width is Lorentzian: $\delta_{vib} = 88\,cm^{-1}$.

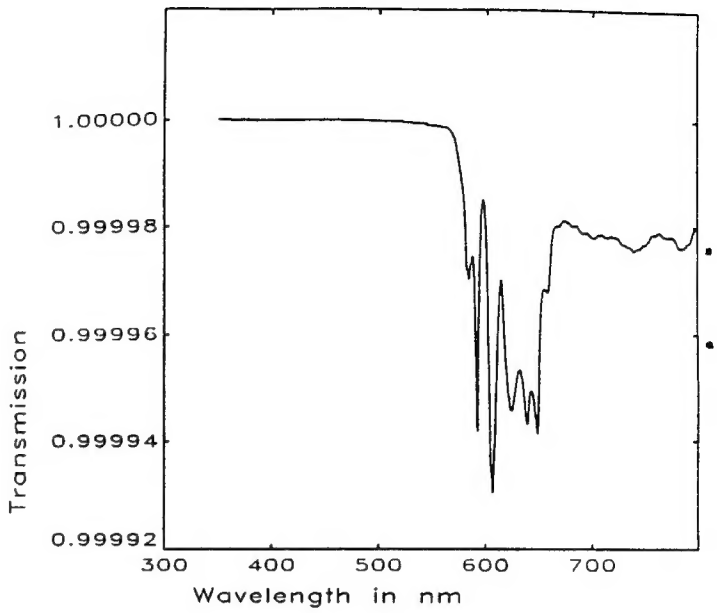

Figure 22—Total vibronic spectrum of diatomic aluminum including the bound-free (X → R) transition modelled by applying the reflection approximation to transition-dipole strengths. $T_{evap}^{Al} = T_{obs} = 2100K$.

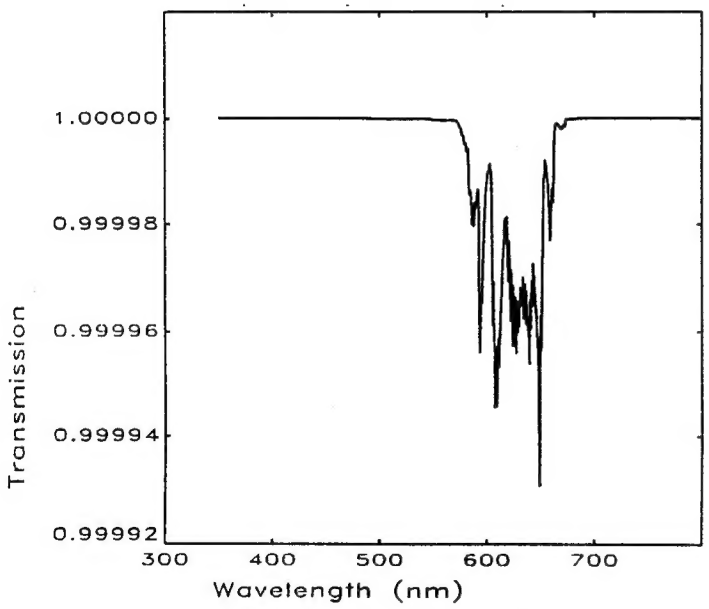

Figure 23—Model rovibronic spectrum of the bound-bound (A → B) transition in diatomic aluminum, combining rotationless transition dipole strengths with rotationally dependent state energies. $T_{evap}^{Al} = T_{obs} = 2100K$. $\delta_{press} = 1.0\,cm^{-1}$ and $\gamma_{instr} = 0.5$ nm.

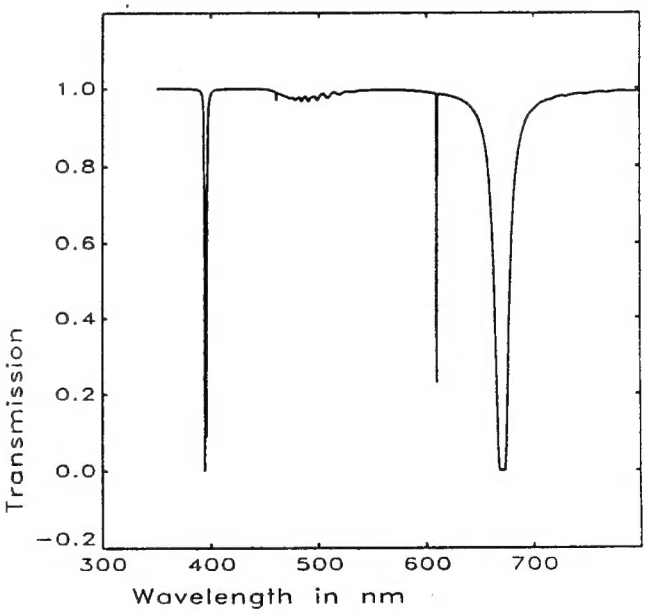

Figure 24—Full-scale broadened vibronic spectrum of the lithium-aluminum system without the heteronuclear contribution. $T_{evap}^{Li} = 1350$ and $T_{evap}^{Al} = T_{obs} = 2100K$. Lorentzian widths: $\delta_{press}^{Li} = 1.5\,cm^{-1}$, $\delta_{press}^{Al} = 1.5\,cm^{-1}$, $\delta_{press}^{Li_2} = 1.0\,cm^{-1}$, and $\delta_{press}^{Al_2} = 1.0\,cm^{-1}$ and Gaussian width: $\gamma_{instr} = 0.5$ nm.

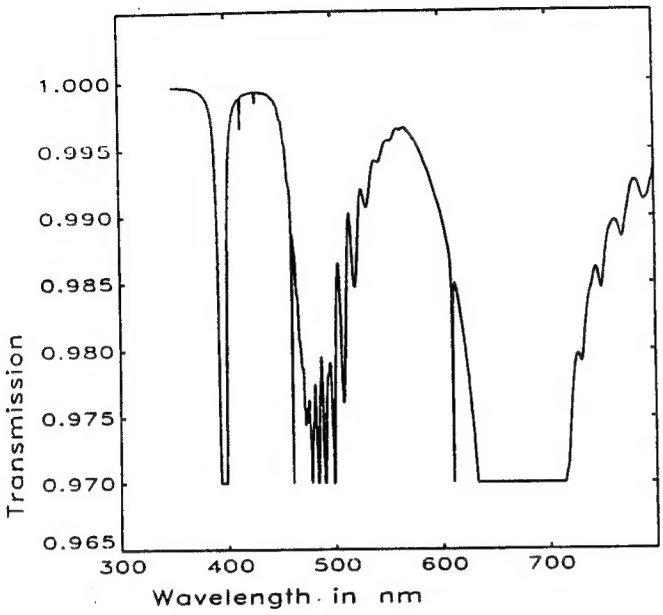

Figure 25—The same vibronic spectrum shown in Figure 24, but on an expanded vertical scale.